current, co-transfection of the mutant did not affect the expressed current densities after depolarizing the test pulse to +40 mV. In contrast, the tail current densities of 1 μg WT were significantly larger ($p<0.05$) than those of WT plus 0.5 μg, 1 μg and 1.5 μg W248F after depolarizing the test pulse to 0 mV, 10 mV and 20 mV.

Recent studies demonstrated that *KCNQ1* mutations in the intracellular S4-S5 linker affected the voltage sensitivity of the reconstituted channels[19] Fig 3C represents the voltage-dependence of current activation. Tail current densities after each test potential were fitted to *Eqn 1* (see methods). The parameters were $V_{1/2}$=+25.4±4.0 mV, k=11.8±0.7 mV for 1 μg WT, $V_{1/2}$=+25.1±2.5 mV, k=11.8±1.3 mV for 0.5 μg WT, $V_{1/2}$=+40.0±2.5 mV, k=12.2±0.5 mV for 0.5 μg WT plus 0.5 μg W248F, $V_{1/2}$=+40.4±1.9 mV, k=12.8±0.5 mV for 0.5 μg WT plus 1 μg W248F, and $V_{1/2}$=+46.2±3.8 mV, k=12.3±0.6 mV for 0.5 μg WT plus 1.5 μg W248F. There was a significant difference in half activation voltages between WT (0.5 and 1 μg) and WT plus W248F (0.5, 1, and 1.5 μg), but no significant difference in slope factors. In other words, the W248F-KCNQ1 affected the WT-KCNQ1 to produce a I_{Ks} channel, but the effects of those to the outward I_{Ks} currents were small. Thus, the W248F-KCNQ1 displayed a small dominant-negative effect.

The W248F-KCNQ1 plus KCNE1 channel displayed very small outward currents at depolarization to +60 mV (eg, original traces of Fig 3A). We further applied non-physiological depolarizing step pulses in another set of experiments on CHO cells expressing the W248F-KCNQ1 I_{Ks} channel. The left panel of Fig 4A depicts a typical current trace. Strong and unphysiological depolarization to +80～+120 mV could elicit ample outward currents with extremely rapid deactivation (Fig 4A, Right). In multiple cells, we analyzed tail current densities and plotted them against the test potential in Fig 4B. To show the current-voltage relationship (Fig 4C), normalized tail current densities were plotted as a function of the test potential and fitted by *Eqn 1* (see methods). $V_{1/2}$ and k values were 94.0±2.7 mV and 8.0±1.1 mV, respectively. Thus, the W248F mutant in the S4-S5 linker of KCNQ1 appeared to cause the I_{Ks} channel a considerable positive shift of activation curves and thereby produced practically no outward currents in the physiological range of membrane potential.

Discussion

In the present study, we described a Japanese family with JLN syndrome. In the proband, we identified a *KCNQ1* homozygous mutation (W248F) and in 3 family members, a heterozygous mutation. All the relatives showed normal QTc intervals without clinical manifestations of LQTS, showing no obvious penetrance.

Phenotype and Penetrance in LQTS

In 1997, Neyroud et al demonstrated 3 affected children from 2 JLN families and first detected the homozygosity for a novel deletion-insertion event in the C-terminal domain of *KCNQ1*[8] The QTc intervals of the heterozygous family members showed a wide range of variations from 365 to 484 ms, but none of them was symptomatic. Splawski et al characterized a single, large JLN family in which deafness was found only in an infant proband with a homozygous 1-bp insertion in the S2-S3 linker of the gene[9] In contrast to the preceding report, extended family surveys revealed that the proband's mother experienced a sudden death, and 14 family members had significantly prolonged QTc intervals; including 6 with a history of syncope[9]

Table 1 summarizes the reported cases of JLN syndrome and their family members with *KCNQ1* mutations. The intervals of QTc in heterozygous mutation carriers varied considerably, ranging from under 400 ms to over 500 ms depending on the mutations and carriers. In contrast, cardiac symptoms were recorded only in the carriers with 2 types of mutations. One of the mutations was the 567 insert G with frameshift at the S2-S3 linker. The details concerning the symptoms are described above[9] Another mutation was the 572-576 deletion with frameshift[20] Among the deletion mutation carriers, only 1 of the 13 heterozygotes experienced syncope.

In general, therefore, heterozygous carriers of the JLN mutation were asymptomatic or mildly symptomatic, although homozygous or compound heterozygous probands usually suffer from severe cardiac events[3] This might be caused by the low penetrance of the JLN-related *KCNQ1* mutations in heterozygous conditions (approximately 30%)[21] Schwartz et al suggested that most of the JLN-related *KCNQ1* mutations might not exert dominant negative effects on the expression of WT *KCNQ1*[3] Indeed, approximately 60% of *KCNQ1* mutations in JLN syndrome are complex mutations like insertion, deletion and nonsense mutations, which under normal circumstances are unable to cause dominant negative suppression because they cannot make an assembly with wild-type normal subunits. In contrast, most of the *KCNQ1* mutations identified in Romano-Ward syndrome are missense mutations[22] which can co-assemble with normal subunits and thereby exert the dominant negative suppression effect.

Mutations in W248 Residue Alter the Gating Properties of the I_{Ks} Channel

W248F-KCNQ1 plus KCNE1 channels produced very small currents by themselves in the physiological range of membrane potential. Franqueza et al reported a W248R-KCNQ1 mutation; the same position as our mutation but a different amino acid change[19] Without KCNE1, the W248R-KCNQ1 channel produced reduced current densities compared to WT-KCNQ1 and displayed no dominant negative effect. And the co-expression of mutant KCNQ1 with KCNE1 caused a marked suppression of I_{Ks} current. We could not compare the results with ours because they performed their functional analysis using *Xenopus* oocytes and the stimulation protocol was different. Both of the mutations, however, displayed extremely smaller I_{Ks} currents. Although we did not perform the analysis without KCNE1, these results prove that the W248 residue is indispensable in co-assembly with KCNE1 and the mutations in this residue decrease the I_{Ks} currents. Considering the similarities of tryprophan and phenylalanine, they are the same amino acids group with non-polar side chains, but the side chains are slightly different; tryptophan has an indole side chain, phenylalanine has a benzyl side chain. In the KCNQ1 S4-S5 linker, a slight amino acid change caused the dynamic change of channel properties; E261D-KCNQ1+KCNE1 channels displayed a marked current decrease[20] although both amino acids have acidic side chains. Thus, amino acid substitution in the S4-S5 linker of KCNQ1 can change channel properties if the substituted amino acids have similar characters.

A Mutant W248F I_{Ks} Channel and Heterozygous Family Members

When co-expressed with WT-KCNQ1 subunits, W248F-KCNQ1 I_{Ks} channels exerted small dominant negative effects. These results imply that the W248F-KCNQ1 I_{Ks} channel subunits can slightly affect the normal subunits. On account of this phenomenon, the heterozygous family members of our proband remained asymptomatic with normal QTc intervals. The expression level of both WT and mutant alleles is controlled in various ways[23] and we need to confirm the protein expression in myocytes to discuss the phenotype of heterozygous family members. But if we assume that both mutant and alleles are translated equally, heterozygous family members are at risk of developing life-threatening arrhythmias in the presence of some triggering factors to prolong the QT interval. This is because their cardiac repolarizing I_{Ks} currents or repolarization reserve[24] would be smaller than those of healthy individuals.

Conclusion

The present study strengthens the notion that asymptomatic family members related to JLN syndrome patients might be heterozygous carriers of the disease-related gene mutations and they would be at risk of lethal arrhythmias in the presence of compounding factors. The functional analysis of a mutant W248F-KCNQ1 channel revealed that the channel did not work in physiological states, and then JLN syndrome is induced because of the non-functional I_{Ks} channel. However, heterozygous mutation carriers are asymptomatic because of the mutant displays very small dominant-negative effects. Therefore, it is of clinical importance to identify such asymptomatic heterozygous mutation carriers to prevent sudden and unexpected cardiac death.

Acknowledgments

The authors wish to express thanks to the proband and her family members for participating in this study; and to Dr J Barhanin (Institut de Pharmacologie Moléculaire et Cellulaire, CNRS, Valvonne, France) for KCNQ1 (GenBank AF000571) and KCNE1 (GenBank M26685) cDNA clones. We also would like to thank Mr R Kaszynski for reading the manuscript.

Minoru Horie was supported by research grants from the Japan Ministry of Education, Science, Sports and Culture and by Health Science Research Grants from the Japan Ministry of Health, Labor and Welfare.

References

1. Horie M, Itoh H. Disorders of cardiac repolarization-long QT and short QT syndromes. *Circ J* 2007; **71**(Supple A): A-50–A-53.
2. Schwartz PJ, Periti M, Malliani A. The long Q-T syndrome. *Am Heart J* 1975; **89:** 378–390.
3. Schwartz PJ, Spazzolini C, Crotti L, Bathen J, Amlie JP, Timothy K, et al. The Jervell and Lange-Nielsen syndrome: Natural history, molecular basis, and clinical outcome. *Circulation* 2006; **113:** 783–790.
4. Jervell A, Lange-Nielsen F. Congenital deaf-mutism, functional heart disease with prolongation of the Q-T interval and sudden death. *Am Heart J* 1957; **54:** 59–68.
5. Roden DM, Lazzara R, Rosen M, Schwartz PJ, Towbin J, Vincent GM. Multiple mechanisms in the long-QT syndrome: Current knowledge, gaps, and future directions: The SADS Foundation Task Force on LQTS. *Circulation* 1996; **94:** 1996–2012.
6. Fraser GR, Froggatt P, James TN. Congenital deafness associated with electrocardiographic abnormalities, fainting attacks and sudden death: A recessive syndrome. *Q J Med* 1964; **33:** 361–385.
7. Jervell A, Thingstad R, Endsjo TO. The surdo-cardiac syndrome: Three new cases of congenital deafness with syncopal attacks and Q-T prolongation in the electrocardiogram. *Am Heart J* 1966; **72:** 582–593.
8. Neyroud N, Tesson F, Denjoy I, Leibovici M, Donger C, Barhanin J, et al. A novel mutation in the potassium channel gene *KVLQT1* causes the Jervell and Lange-Nielsen cardioauditory syndrome. *Nat Genet* 1997; **15:** 186–189.
9. Splawski I, Timothy KW, Vincent GM, Atkinson DL, Keating MT. Molecular basis of the long-QT syndrome associated with deafness. *N Engl J Med* 1997; **336:** 1562–1567.
10. Schulze-Bahr E, Wang Q, Wedekind H, Haverkamp W, Chen Q, Sun Y, et al. *KCNE1* mutations cause Jervell and Lange-Nielsen syndrome. *Nat Genet* 1997; **17:** 267–268.
11. Duggal P, Vesely MR, Wattanasirichaigoon D, Villafane J, Kaushik V, Beggs AH. Mutation of the gene for IsK associated with both Jervell and Lange-Nielsen and Romano-Ward forms of Long-QT syndrome. *Circulation* 1998; **97:** 142–146.
12. Barhanin J, Lesage F, Guillemare E, Fink M, Lazdunski M, Romey G. KvLQT1 and IsK (minK) proteins associate to form the I_{Ks} cardiac potassium current. *Nature* 1996; **384:** 78–80.
13. Sanguinetti MC, Curran ME, Zou A, Shen J, Spector PS, Atkinson DL, et al. Coassembly of KvLQT1 and minK (IsK) proteins to form cardiac I_{Ks} potassium channel. *Nature* 1996; **384:** 80–83.
14. Ohno S, Zankov DP, Yoshida H, Tsuji K, Makiyama T, Itoh H, et al. N- and C-terminal KCNE1 mutations cause distinct phenotypes of long QT syndrome. *Heart Rhythm* 2007; **4:** 332–340.
15. Mohler PJ, Schott JJ, Gramolini AO, Dilly KW, Guatimosim S, duBell WH, et al. Ankyrin-B mutation causes type 4 long-QT cardiac arrhythmia and sudden cardiac death. *Nature* 2003; **421:** 634–639.
16. Vatta M, Ackerman MJ, Ye B, Makielski JC, Ughanze EE, Taylor EW, et al. Mutant caveolin-3 induces persistent late sodium current and is associated with long-QT syndrome. *Circulation* 2006; **114:** 2104–2112.
17. Medeiros-Domingo A, Kaku T, Tester DJ, Iturralde-Torres P, Itty A, Ye B, et al. SCN4B-encoded sodium channel beta4 subunit in congenital long-QT syndrome. *Circulation* 2007; **116:** 134–142.
18. Wang Q, Curran ME, Splawski I, Burn TC, Millholland JM, VanRaay TJ, et al. Positional cloning of a novel potassium channel gene: KVLQT1 mutations cause cardiac arrhythmias. *Nat Genet* 1996; **12:** 17–23.
19. Franqueza L, Lin M, Shen J, Splawski I, Keating MT, Sanguinetti MC. Long QT syndrome-associated mutations in the S4-S5 linker of KvLQT1 potassium channels modify gating and interaction with minK subunits. *J Biol Chem* 1999; **274:** 21063–21070.
20. Huang L, Bitner-Glindzicz M, Tranebjaerg L, Tinker A. A spectrum of functional effects for disease causing mutations in the Jervell and Lange-Nielsen syndrome. *Cardiovasc Res* 2001; **51:** 670–680.
21. Priori SG, Napolitano C, Schwartz PJ. Low penetrance in the long-QT syndrome: Clinical impact. *Circulation* 1999; **99:** 529–533.
22. Tester DJ, Will ML, Haglund CM, Ackerman MJ. Compendium of cardiac channel mutations in 541 consecutive unrelated patients referred for long QT syndrome genetic testing. *Heart Rhythm* 2005; **2:** 507–517.
23. Rosati B, McKinnon D. Regulation of ion channel expression. *Circ Res* 2004; **94:** 874–883.
24. Roden DM. Taking the "idio" out of "idiosyncratic": Predicting torsades de pointes. *Pacing Clin Electrophysiol* 1998; **21:** 1029–1034.
25. Chen Q, Zhang D, Gingell RL, Moss AJ, Napolitano C, Priori SG, et al. Homozygous deletion in *KVLQT1* associated with Jervell and Lange-Nielsen syndrome. *Circulation* 1999; **99:** 1344–1347.
26. Splawski I, Shen J, Timothy KW, Lehmann MH, Priori S, Robinson JL, et al. Spectrum of mutations in long-QT syndrome genes: *KVLQT1, HERG, SCN5A, KCNE1,* and *KCNE2*. *Circulation* 2000; **102:** 1178–1185.
27. Zehelein J, Kathoefer S, Khalil M, Alter M, Thomas D, Brockmeier K, et al. Skipping of exon 1 in the KCNQ1 gene causes Jervell and Lange-Nielsen syndrome. *J Biol Chem* 2006; **281:** 35397–35403.
28. Chouabe C, Neyroud N, Richard P, Denjoy I, Hainque B, Romey G, et al. Novel mutations in KvLQT1 that affect I_{Ks} activation through interactions with Isk. *Cardiovasc Res* 2000; **45:** 971–980.
29. Piippo K, Swan H, Pasternack M, Chapman H, Paavonen K, Viitasalo M, et al. A founder mutation of the potassium channel KCNQ1 in long QT syndrome: Implications for estimation of disease prevalence and molecular diagnostics. *J Am Coll Cardiol* 2001; **37:** 562–568.
30. Wang Z, Li H, Moss AJ, Robinson J, Zareba W, Knilans T, et al. Compound heterozygous mutations in *KvLQT1* cause Jervell and Lange-Nielsen syndrome. *Mol Genet Metab* 2002; **75:** 308–316.
31. Tyson J, Tranebjaerg L, Bellman S, Wren C, Taylor JF, Bathen J, et al. IsK and KvLQT1: Mutation in either of the two subunits of the slow component of the delayed rectifier potassium channel can cause Jervell and Lange-Nielsen syndrome. *Hum Mol Genet* 1997; **6:** 2179–2185.
32. Tranebjaerg L, Bathen J, Tyson J, Bitner-Glindzicz M, Jervell and Lange-Nielsen syndrome: A Norwegian perspective. *Am J Med Genet*

1999; **89:** 137–146.
33. Tyson J, Tranebjaerg L, McEntagart M, Larsen LA, Christiansen M, Whiteford ML, et al. Mutational spectrum in the cardioauditory syndrome of Jervell and Lange-Nielsen. *Hum Genet* 2000; **107:** 499–503.
34. Neyroud N, Denjoy I, Donger C, Gary F, Villain E, Leenhardt A, et al. Heterozygous mutation in the pore of potassium channel gene *KvLQT1* causes an apparently normal phenotype in long QT syndrome. *Eur J Hum Genet* 1998; **6:** 129–133.
35. Wei J, Fish FA, Myerburg RJ, Roden DM, George AL Jr. Novel *KCNQ1* mutations associated with recessive and dominant congenital long QT syndromes: Evidence for variable hearing phenotype associated with R518X. *Hum Mutat* 2000; **15:** 387–388.
36. Ning L, Moss AJ, Zareba W, Robinson J, Rosero S, Ryan D, et al. Novel compound heterozygous mutations in the KCNQ1 gene associated with autosomal recessive long QT syndrome (Jervell and Lange-Nielsen syndrome). *Ann Noninv Electrocard* 2003; **8:** 246–250.
37. Neyroud N, Richard P, Vignier N, Donger C, Denjoy I, Demay L, et al. Genomic organization of the *KCNQ1* K^+ channel gene and identification of C-terminal mutations in the long-QT syndrome. *Circ Res* 1999; **84:** 290–297.

Journal of the American College of Cardiology
© 2008 by the American College of Cardiology Foundation
Published by Elsevier Inc.

Vol. 52, No. 16, 2008
ISSN 0735-1097/08/$34.00
doi:10.1016/j.jacc.2008.07.013

A Novel *SCN5A* Gain-of-Function Mutation M1875T Associated With Familial Atrial Fibrillation

Takeru Makiyama, MD, PHD,* Masaharu Akao, MD, PHD,* Satoshi Shizuta, MD,* Takahiro Doi, MD,* Kei Nishiyama, MD,* Yuko Oka, MD,† Seiko Ohno, MD, PHD,* Yukiko Nishio, MD,* Keiko Tsuji, MS,† Hideki Itoh, MD, PHD,† Takeshi Kimura, MD, PHD,* Toru Kita, MD, PHD,* Minoru Horie, MD, PHD†

Kyoto and Otsu, Japan

Objectives This study describes a novel heterozygous gain-of-function mutation in the cardiac sodium (Na^+) channel gene, *SCN5A*, identified in a Japanese family with lone atrial fibrillation (AF).

Background *SCN5A* mutations have been associated with a variety of inherited arrhythmias, but the gain-of-function type modulation in *SCN5A* is associated with only 1 phenotype, long-QT syndrome type 3 (LQTS3).

Methods We studied a Japanese family with autosomal dominant hereditary AF, multiple members of which showed an onset of AF or frequent premature atrial contractions at a young age.

Results The 31-year-old proband received radiofrequency catheter ablation, during which time numerous ectopic firings and increased excitability throughout the right atrium were documented. Mutational analysis identified a novel missense mutation, M1875T, in *SCN5A*. Further investigations revealed the familial aggregation of this mutation in all of the affected individuals. Functional assays of the M1875T Na^+ channels using a whole-cell patch-clamp demonstrated a distinct gain-of-function type modulation; a pronounced depolarized shift (+16.4 mV) in $V_{1/2}$ of the voltage dependence of steady-state inactivation; and no persistent Na^+ current, which is a defining mechanism of LQTS3. These biophysical features of the mutant channels are potentially associated with increased atrial excitability and normal QT interval in all of the affected individuals.

Conclusions We identified a novel *SCN5A* mutation associated with familial AF. The mutant channels displayed a gain-of-function type modulation of cardiac Na^+ channels, which is a novel mechanism predisposing to increased atrial excitability and familial AF. This is a new phenotype resulting from the *SCN5A* gain-of-function mutations and is distinct from LQTS3. (J Am Coll Cardiol 2008;52:1326–34) © 2008 by the American College of Cardiology Foundation

The cardiac sodium (Na^+) channel plays a crucial role in cardiac excitation/contraction via initiating the action potential of the conduction system and working myocytes. Mutations in *SCN5A*—which encodes the α-subunit of voltage-gated cardiac Na^+ channels—have been associated with a variety of cardiac arrhythmias. The loss-of-function mutations result in Brugada syndrome (1), idiopathic ventricular fibrillation (2), cardiac conduction disease (3), or congenital sick sinus syndrome (4), whereas the gain-of-function type modulation in *SCN5A* is associated with only 1 phenotype, long-QT syndrome type 3 (LQTS3) (5).

We reported on the screening for *SCN5A* mutations in Japanese patients with Brugada syndrome (6) and now have extended the cohort to various inherited arrhythmias, given the wide spectrum of clinical phenotypes of cardiac Na^+ channelopathies. In the present study, in a Japanese family with lone atrial fibrillation (AF), we identified a novel missense mutation of *SCN5A* (M1875T). Until recently, only potassium channel mutations have been linked to familial AF (7–10); however, 3 recent reports have identified *SCN5A* loss-of-function mutations: D1275N in 2 families with atrial arrhythmias (AF, cardiac conduction disease, or sick sinus syndrome) plus dilated cardiomyopathy (11,12), and N1986K in a family with lone AF (13). Thus, this is the first report to identify an *SCN5A* gain-of-function type mutation in familial AF.

From the *Department of Cardiovascular Medicine, Kyoto University Graduate School of Medicine, Kyoto, Japan; and the †Department of Cardiovascular and Respiratory Medicine, Shiga University of Medical Science, Otsu, Japan. This work was supported by research grants from the Japan Heart Foundation/Pfizer Japan Inc. Grant for Research on Cardiovascular Disease; Grants-in-Aid in Scientific Research from the Ministry of Education, Culture, Science, and Technology of Japan; and a Health Sciences Research Grant (H18-Research on human Genome-002) from the Ministry of Health, Labor and Welfare of Japan.

Manuscript received March 3, 2008; revised manuscript received July 7, 2008, accepted July 10, 2008.

Methods

Clinical evaluation. This study was approved by the Institutional Ethics Committee, and all patients provided informed consent. Affected individuals were considered as having AF or premature atrial contractions (PACs) when documented by 12-lead electrocardiograms (ECGs). Lone AF was defined as onset of AF at age <65 years without structural heart disease, hypertension, hyperthyroidism, myocardial infarction, or congestive heart failure. Paroxysmal AF was defined as sporadic AF lasting >30 s for <7 days. When sustained beyond 7 days, AF was considered persistent. Atrial fibrillation refractory to cardioversion or not attempted was classified as permanent. In both sinus rhythm and AF, the mean QT and RR intervals were measured from 3 and 6 consecutive beats, respectively.

Deoxyribonucleic acid (DNA) isolation and mutation analysis. Genomic DNA was isolated from blood lymphocytes and screened for candidate genes by denaturing high-performance liquid chromatography with a WAVE System Model 3500 (Transgenomic, Omaha, Nebraska). Abnormal conformers were amplified by polymerase chain reaction, and sequencing was performed on an ABI PRISM 3100 DNA sequencer (Applied Biosystems, Foster City, California).

Site-directed mutagenesis and electrophysiology. To construct the *SCN5A* mutant, we adopted site-directed mutagenesis performed via a kit, QuickChange II XL (Stratagene, La Jolla, California). The human cell line HEK293 cultured in a 35-mm dish was transiently transfected with 0.5 μg of either pRcCMV-WT or mutant complementary DNA in combination with 0.5 μg of the bicistronic plasmid (pEGFP-IRES-hβ1) encoding enhanced green fluorescent protein and the human β1-subunit (hβ1). The Na^+ currents were recorded 48 h after transfection with the whole-cell patch-clamp technique at 22°C to 23°C as described elsewhere (14). Results are expressed as mean ± SEM, and statistical significance was established with the Student *t* test. Statistical significance was assumed for $p < 0.05$.

Abbreviations and Acronyms

AF = atrial fibrillation
AT = atrial tachycardia
ECG = electrocardiogram
LQTS3 = long-QT syndrome type 3
PAC = premature atrial contraction
WT = wild-type

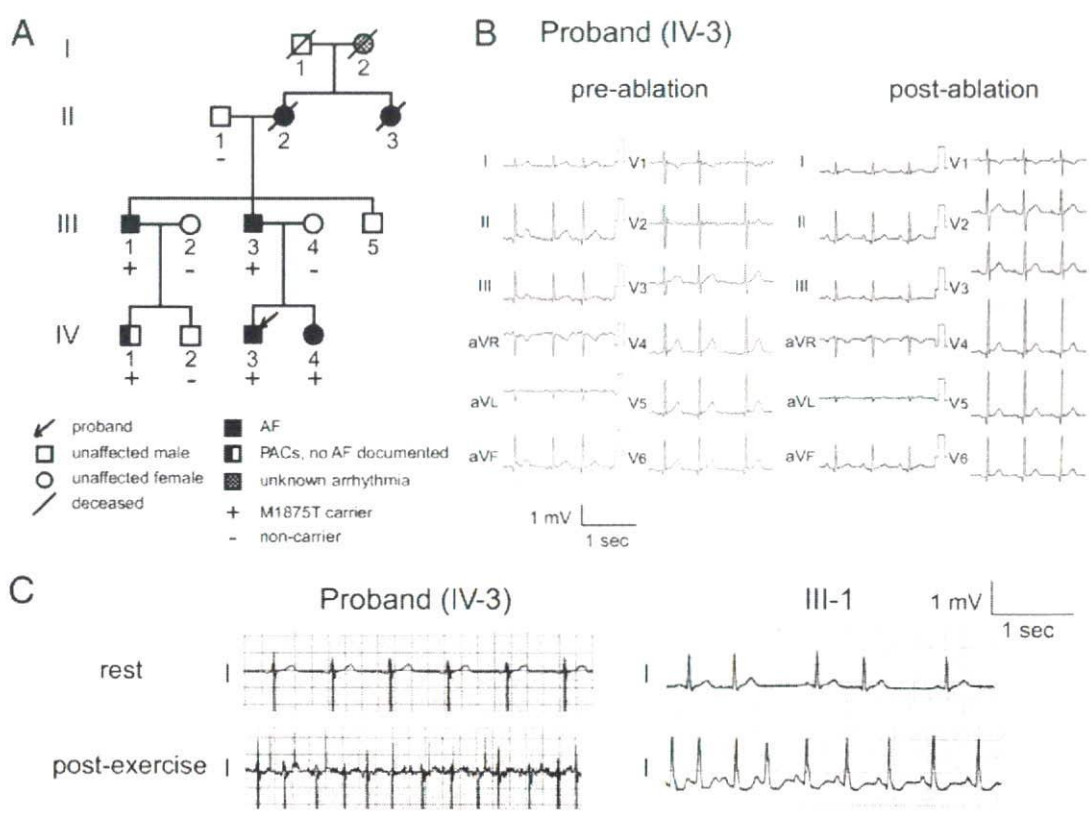

Figure 1 Pedigree and Clinical Features

(A) Pedigree of the family. Phenotypic traits are designated within pedigree symbols. **(B)** Electrocardiograms (ECGs) obtained from the proband, IV-3, before (**left panel**, atrial fibrillation [AF]) and after (**right panel**, sinus rhythm) he underwent radiofrequency catheter ablation. **(C)** At rest and post-exercise ECGs recorded from the proband (IV-3) and his uncle (III-1). Exercise-induced AF for the proband and atrial tachycardia for the uncle can be observed. *Continued on next page.*

JACC Vol. 52, No. 16, 2008
October 14, 2008:1326–34

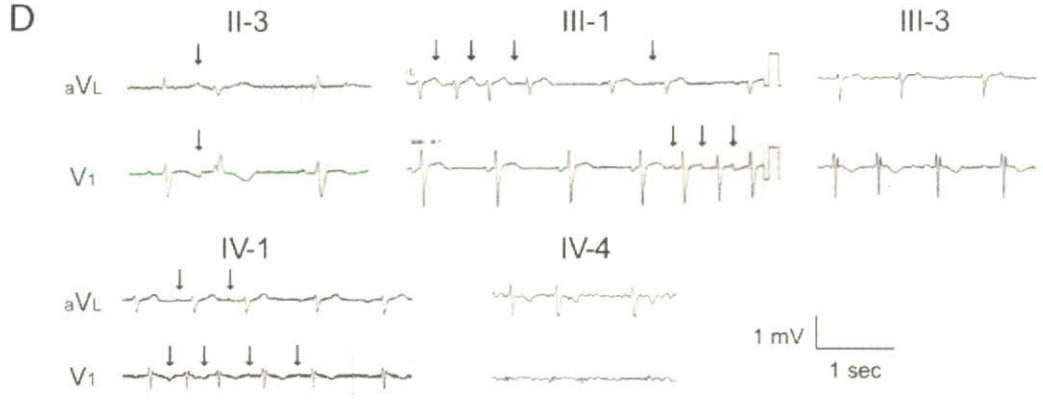

Figure 1 Continued

(D) Electrocardiograms recorded from other affected individuals. **Arrows** indicate P waves of premature atrial contractions (PACs) in II-3, III-1, and IV-1. III-3 and IV-4 demonstrated AF.

Results

Clinical features. We studied a Japanese family with autosomal dominant hereditary AF that spanned 3 generations (Fig. 1A). The proband (IV-3) (Fig. 1A), a 31-year-old man, first experienced repetitive palpitation due to frequent PACs at age 18, which later progressed to paroxysmal AF and atrial tachycardia (AT) at age 27 years (pre-ablation) (Fig. 1B).

Six family members, along with the proband, presented with either AF or frequent PACs (Fig. 1A). The majority shared a similar clinical course with the proband—palpitations due to PACs start in their teens, which later progress to paroxysmal and ultimately persistent AF (Table 1). The proband and his uncle (III-1) showed exercise-induced AT and/or AF (Fig. 1C). The proband's cousin (IV-1) presented with frequent PACs (Fig. 1D) that have not yet progressed to AF. The ECGs of the affected relatives—with the exception to the proband's aunt (II-3), who received disopyramide—did not show any QT prolongation (Fig. 1D, Table 1). Interestingly, the analysis of P wave morphology in the affected family members revealed that the majority of PAC foci were localized in the right atrium (Fig. 1D). The affected individuals received various antiarrhythmic agents (Table 1) but, in most cases, to no avail. There was neither structural heart disease nor a history of major ventricular arrhythmias or sudden cardiac death in this family.

At age 27 years, the proband underwent radiofrequency catheter ablation. Intravenous administration of isoproterenol induced repetitive ATs from multiple origins in the right atrium (Fig. 2A). We successfully ablated the major origin, located in the lower-right atrial septum (Figs. 2B and 2C).

Three years later, the second ablation session was performed due to a relapse of persistent AF. This time, we identified 2 other PAC foci in the right atrium (Fig.

Table 1 Clinical Characteristics of Affected Individuals

Individual	Gender	Age (yrs)	Arrhythmias	Onset of PAC (yrs)	Onset of AF (yrs)	Mutation Carrier	HR (beats/min)	QRS (ms)	QTc	LAD (mm)	LVEF (%)	Antiarrhythmic Agents Used to Treat AF
I-2	F	90*	Unknown	NA	NA	ND	NA	NA	NA	NA	NA	NA
II-2	F	75*	Permanent AF	NA	NA	ND	88	74	427	36	79	—
II-3	F	75*	Paroxysmal AF, PACs	NA	NA	ND	77†	104†	478†	30	75	Disopyramide
III-1	M	60	Paroxysmal AF, PACs	NA	48	Yes	70	92	394	32	75	Disopyramide, cibenzoline, aprindine
III-3	M	57	Permanent AF	15	51	Yes	71	82	385	NA	NA	—
IV-1	M	34	PACs	23	—	Yes	68	82	399	ND	ND	—
IV-3	M	31	Persistent AF	18	27	Yes	65	81	388	30	63	Pilsicainide, flecainide
IV-4	F	29	Permanent AF	12	26	Yes	88	87	429	31	61	Pilsicainide

*Age of death; †disopyramide administration.
AF = atrial fibrillation; HR = heart rate; LAD = left atrial dimension; LVEF = left ventricular ejection fraction; NA = records not available; ND = not determined; PAC = premature atrial contraction.

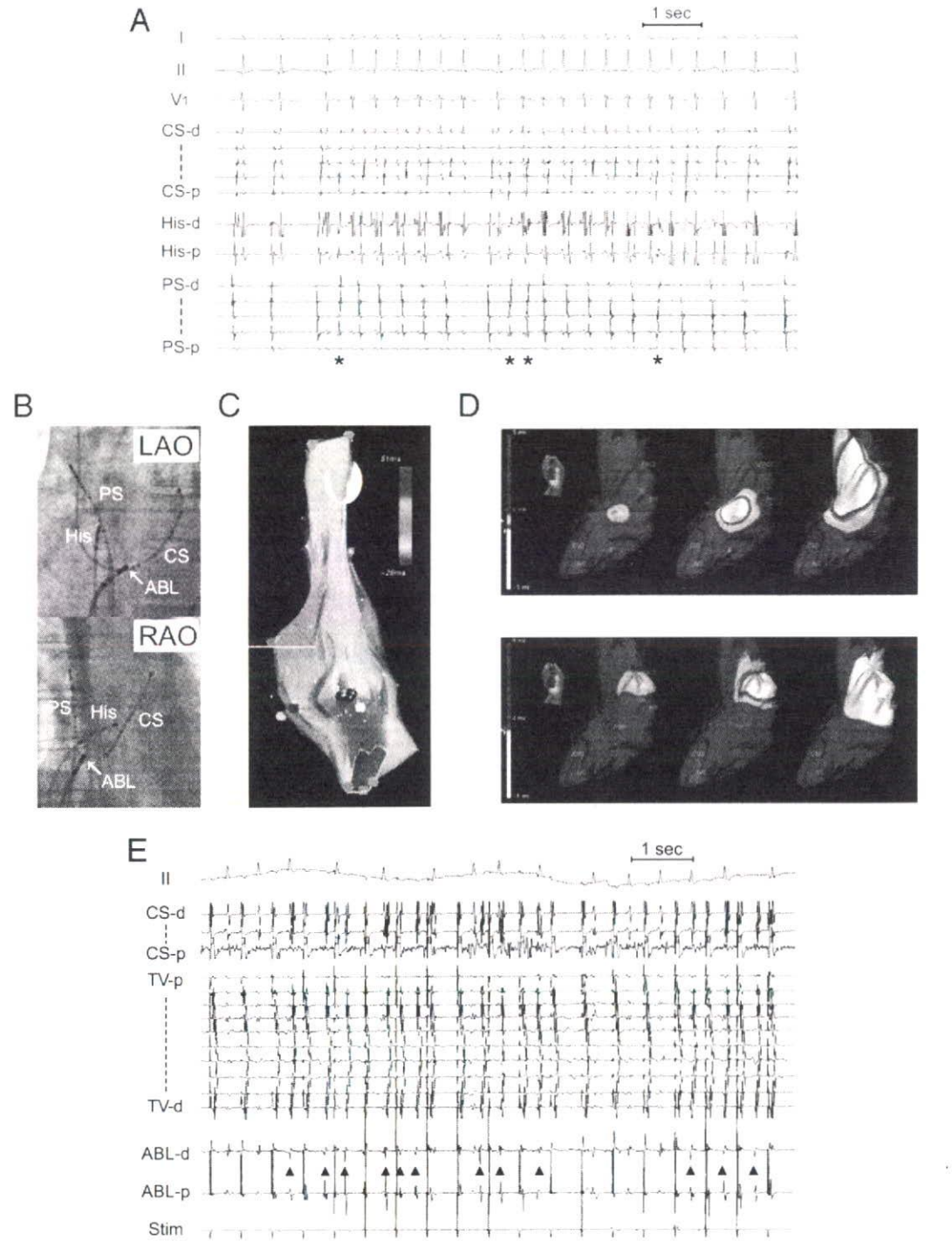

Figure 2 **Radiofrequency Catheter Ablation Recordings**

The first **(A to C)** and the second **(D and E)** ablation sessions on the proband. **(A)** Repetitive atrial tachycardias (ATs) from multiple origins. Shown are intracardiac recordings from the coronary sinus (CS), the His bundle (His), and a catheter placed along the posterior septum (PS) in the right atrium. Note that atrial activation sequences in CS during ATs were consistently proximal to distal, suggesting right atrial origins. **Asterisks** indicate the successfully ablated AT originating from the lower-right atrial septum. **(B)** Fluoroscopic images of the electrodes in the left anterior oblique (LAO) and right anterior oblique (RAO) views. Position of the ablation catheter (ABL; indicated by **arrows**); successful ablation site of the AT. **(C)** Three-dimensional electroanatomic map of the AT in the right posterior oblique view. The AT focus in the lower-right atrial septum was successfully ablated in the first session. **(D)** Noncontact mapping of PACs in the right lateral view. Two PAC foci in the middle of the crista terminalis **(upper panel)** and the high posterolateral wall **(lower panel)** ablated successfully in the second session are shown. **(E)** Numerous electrical firings (▲) from the contact site during radiofrequency energy delivery in generating tricuspid valve isthmus block. Continuous pacing was performed from proximal CS. Stim = stimulator; TV = tricuspid valve annulus; other abbreviations as in Figure 1.

JACC Vol. 52, No. 16, 2008
October 14, 2008:1326–34

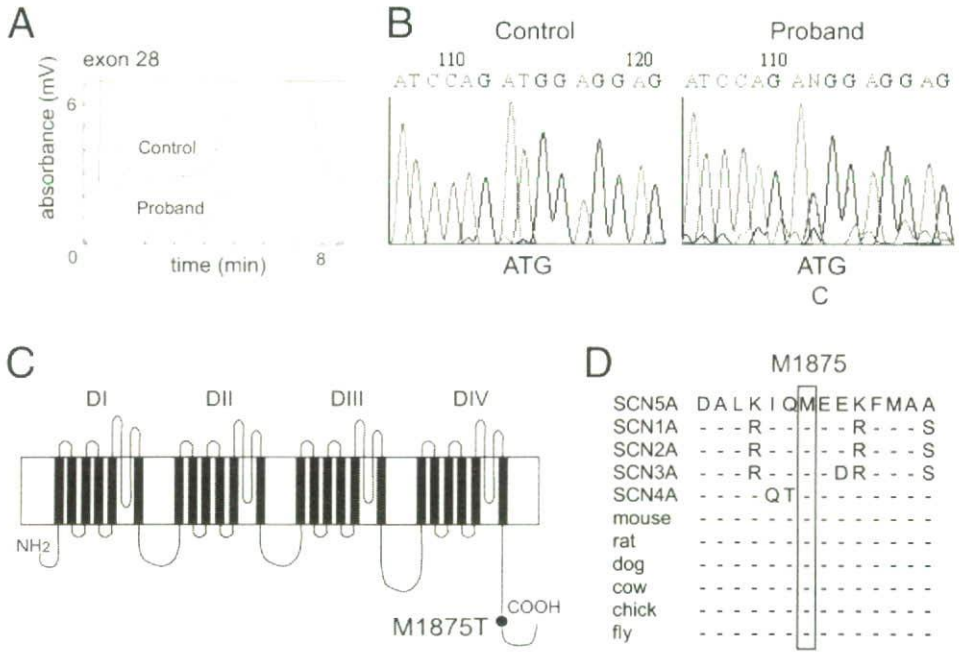

Figure 3 **Genetic Analysis**

(A) The denaturing high-performance liquid chromatography elution profiles for an *SCN5A* mutation, M1875T, detected in the affected family members. **(B)** Deoxyribonucleic acid sequencing electropherograms demonstrate heterozygosity for a *SCN5A* mutation. **(C)** Topology of the α-subunit of voltage-gated cardiac sodium (Na^+) channel. The location of the detected mutation is shown. **(D)** Amino acid sequence alignments of *SCN5A* with related Na^+ channels. The *SCN5A* indicates human heart; *SCN1A*, human brain type I; *SCN2A*, human brain type II; *SCN3A*, human brain type III; *SCN4A*, human skeletal muscle. The sequences of other species represent the cardiac isoforms of Na^+ channels.

2D)—both were successfully ablated. During the subsequent procedure to generate a cavotricuspid isthmus block, we noticed that energy delivery from the catheter induced numerous electrical firings from the contact sites (Fig. 2E). After the second ablation session, he maintained a sinus rhythm under medication, yet even after which he experienced occasional episodes of paroxysmal AF. Interestingly, after each attempt of cardioversion, ATs that lasted for several seconds were observed immediately after the shock was delivered and before sinus rhythm conversion (data not shown). All of these features strongly suggest the proband's increased vulnerability to atrial arrhythmias.

Genetic analysis. We identified a novel missense mutation, c.5624T>C, p.M1875T, in the *SCN5A* gene in the proband. Figure 3 shows the denaturing high-performance liquid chromatography and sequence results (Figs. 3A and 3B) and an illustration showing the position of the identified mutation (Fig. 3C). The amino acid at codon 1875 (methionine) is highly conserved among different Na^+ channel isoforms and species (Fig. 3D). Furthermore, this mutation was absent in 210 Japanese control individuals (420 chromosomes). We failed to identify mutations in any other potential candidate genes of familial AF (*KCNQ1*, *KCNH2*, *KCNE1*, *KCNE2*, *KCNE3*, *KCNJ2*, and *KCNA5*). Further analysis of the family members revealed that the M1875T mutation in SCN5A perfectly matched their clinical phenotypes (Figs. 1A and 1D, Table 1).

Functional analysis of M1875T-*SCN5A*. We performed biophysical assays for the novel *SCN5A* mutation with a heterologous expression system in HEK293 cells. Figure 4A illustrates representative whole-cell current traces from cells expressing wild-type (WT) and M1875T Na^+ channels in the presence of the coexpressed Na^+ channel β subunit.

Notably, M1875T channels showed an apparently slower inactivation compared with WT. The time constants for both fast and slow inactivation across a wide range of test potentials were significantly larger with M1875T in comparison with WT (Fig. 4B), indicating impaired inactivation. Figure 4C shows the peak current-voltage relation for WT and M1875T channels. The maximum current density of WT was observed at −20 mV but shifted to −30 mV for M1875T. In addition, the peak current density of M1875T was significantly larger than WT (WT, 326.2 ± 28.2 pA/pF, n = 23; M1875T, 484.6 ± 49.6 pA/pF, n = 31, $p < 0.01$) (Fig. 4D). As in WT, M1875T channels showed no persistent inward Na^+ currents at the end of a 200-ms depolarization (Fig. 4E), which is one of the defining mechanisms of QT interval prolongation in patients with LQTS3. The subtracted amplitude at the end of the 200-ms depolarization was 0.046 ± 0.009% (n = 5) of the peak current for WT and 0.048 ± 0.038% (n = 7) for M1875T.

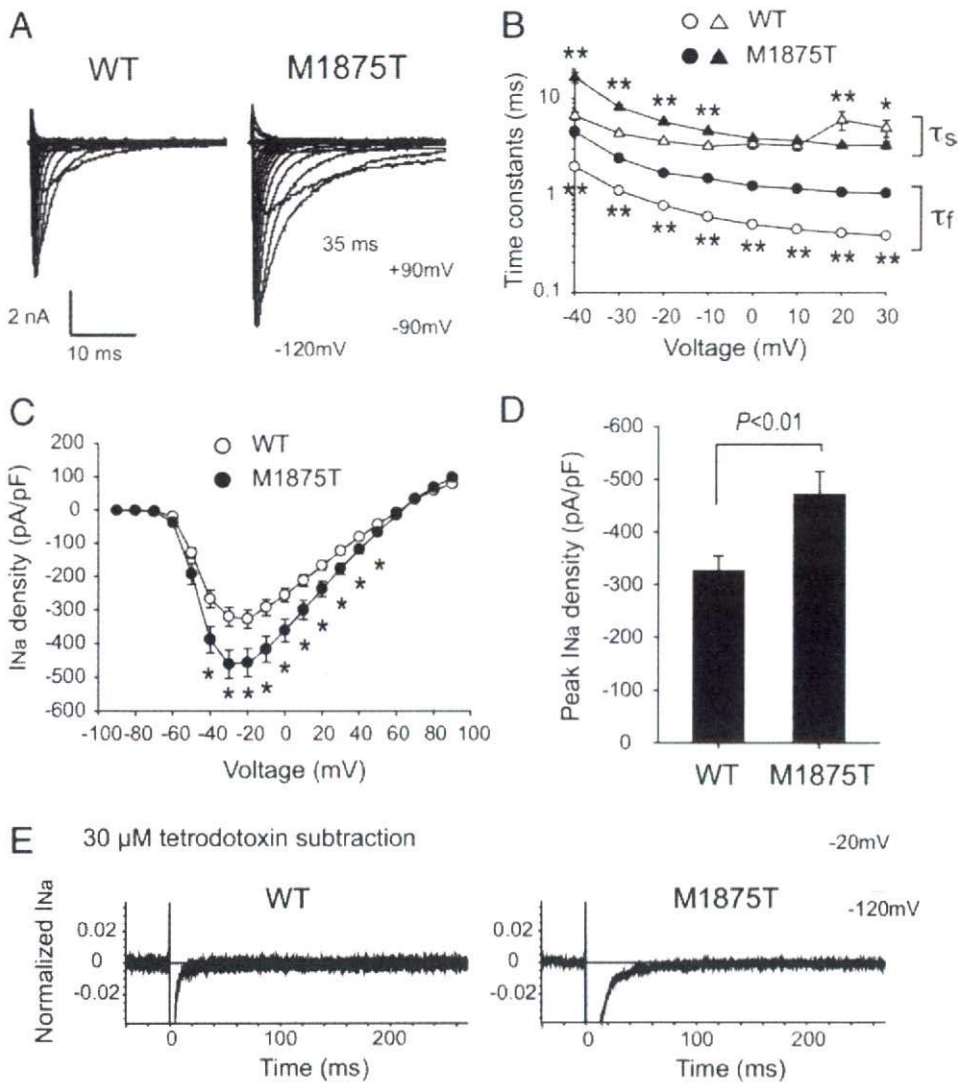

Figure 4 **Macroscopic Na^+ Currents of M1875T Channels**

(A) Representative whole-cell current traces of wild-type (WT) and M1875T sodium (Na^+) channels. Cells were transfected with human β1-subunit (protocol shown as an inset). **(B)** Voltage dependence of inactivation time constants. The time course of inactivation was fit with a 2 exponential equation: $I/I_{max} = A_f \times \exp(-t/\tau_f) + A_s \times \exp(-t/\tau_s)$. Lower and upper bundles of symbols indicate fast (τ_f) and slow (τ_s) time constant values, respectively. Statistically significant differences are indicated (*$p < 0.05$, **$p < 0.01$). **(C)** Average current-voltage relationship for WT and M1875T channels. The current is normalized to cell capacitance to give a measure of Na^+ current density. **Asterisks** indicate the voltages at which the current density was statistically different (*$p < 0.05$). **(D)** Average peak Na^+ current density of WT and M1875T channels. The peak current density was significantly larger in M1875T (WT at −20 mV, 326.2 ± 28.2 pA/pF, n = 23; M1875T at −30 mV, 484.6 ± 49.6 pA/pF, n = 31, $p < 0.05$). **(E)** Representative Na^+ current traces recorded in the absence or presence of 30 μmol/l tetrodotoxin. Tetrodotoxin-sensitive persistent currents were calculated by digital subtraction. M1875T channels showed no persistent inward Na^+ currents.

Figure 5A shows the conductance-voltage and steady-state inactivation curves for WT and M1875T channels. Numerical data pertaining to the biophysical properties therein are summarized in Table 2. The parameters for the activation gate were similar between WT and M1875T. In contrast, the half-maximal potential ($V_{1/2}$) for the steady-state inactivation of M1875T showed a marked positive shift (+16.4 mV) compared with that of WT (WT, $V_{1/2} = -78.08 \pm 0.94$ mV, n = 22; M1875T, $V_{1/2} = -61.68 \pm 0.76$ mV, n = 33, $p < 0.01$). The slope factor (k) for M1875T was significantly larger than that of WT (WT, $k = -7.13 \pm 0.12$, n = 22; M1875T, $k = -6.07 \pm 0.16$, n = 33, $p < 0.01$). The pronounced depolarizing shift of the inactivation gate is likely to increase Na^+ channel availability during excitation.

We also investigated the other kinetic properties of Na^+ channels: recovery from inactivation, onset of slow inactivation, and closed-state inactivation. Parameters of recovery from inactivation and onset of slow inactivation were identical between WT and M1875T (Figs. 5B and 5C,

Table 2 Biophysical Properties of WT and M1875T Channels

	WT	M1875T
Activation (mV)	(n = 23)	(n = 37)
$V_{1/2}$	−43.61 ± 0.79	−44.09 ± 0.72
k	6.53 ± 0.16	5.98 ± 0.18
Steady-state inactivation (mV)	(n = 22)	(n = 33)
$V_{1/2}$	−78.08 ± 0.94	−61.68 ± 0.76†
k	−7.13 ± 0.12	−6.07 ± 0.16†
Recovery from inactivation	(n = 16)	(n = 25)
A_f	0.84 ± 0.01	0.84 ± 0.01
A_s	0.15 ± 0.01	0.15 ± 0.01
τ_f (ms)	8.95 ± 0.95	8.32 ± 0.83
τ_s (ms)	338.6 ± 30.4	271.6 ± 31.6
Onset of slow inactivation	(n = 15)	(n = 16)
A	0.12 ± 0.01	0.12 ± 0.01
τ (ms)	773.9 ± 90.0	647.2 ± 70.6
Closed-state inactivation	(n = 9)	(n = 9)
A	0.13 ± 0.03	0.05 ± 0.02*
τ (ms)	97.1 ± 7.8	212.7 ± 22.3†

Data are mean ± SEM. Parameters were obtained from fitting individual experiments illustrated in Figure 4. *p < 0.05; †p < 0.01 versus wild-type (WT).

A and τ = fractional amplitude and time constant, respectively; n = number of tested cells; $V_{1/2}$ and k = midpoint potential and slope factor, respectively.

Table 2). With regard to closed-state inactivation, the extent was significantly less (WT, A = 0.13 ± 0.03 ms, n = 9; M1875T, A = 0.05 ± 0.02 ms, n = 9, $p < 0.05$), and the time constant was larger in the M1875T channels when compared with WT (WT, τ = 97.1 ± 7.8 ms, n = 9; M1875T, τ = 212.7 ± 22.3 ms, n = 9, $p < 0.01$) (Fig. 5D, Table 2). These data suggest that the number of inactivated M1875T channels is reduced near the resting potential.

Collectively, the M1875T mutation exhibited a gain-of-function type modulation in the cardiac Na^+ channels without persistent inward Na^+ currents: increased peak Na^+ channel density; prolonged time constants of both fast and slow inactivation; a large depolarizing shift in $V_{1/2}$ of the steady-state inactivation; and a lesser extent and a larger time constant with regard to closed-state inactivation. In short, the M1875T mutation clearly demonstrates characteristics that make it distinct from the LQTS3-type gain-of-function modulation.

Discussion

In the present study, we identified a novel gain-of-function *SCN5A* mutation that causes a familial form of AF. The clinical course of AF development materialized in a similar fashion among all affected family members (i.e., palpitations due to frequent PACs and ATs in their teens, followed by paroxysmal and then persistent AF). During the clinical electrophysiological study in the proband, we recognized multifocal activity sites and increased excitability in the right atrium. These distinguishing features are presumably associated with the unique biophysical properties of the mutant Na^+ channels. It should be noted, however, that the size of the pedigree analyzed in this study is limited.

***SCN5A* mutations and familial AF.** Mutations in *SCN5A* have been reported to cause a wide variety of cardiac arrhythmias. The gain-of-function mutations result in LQTS3 (5), whereas the loss-of-function mutations result in various phenotypes: 1) Brugada syndrome; 2) idiopathic ventricular fibrillation; 3) cardiac conduction disease; and 4) congenital sick sinus syndrome. We previously reported that *SCN5A*-linked Brugada syndrome is a high-risk group of bradyarrhythmias, linked predominantly to sick sinus syndrome (6). Although AF is a common complication of Brugada syndrome (10% to 30%) (6,15), there is a scarcity of reports on *SCN5A*-positive Brugada syndrome and AF.

Atrial fibrillation is the most common form of cardiac arrhythmia, characterized by rapid irregular activation of the atrium, and a common cause of morbidity and mortality. Atrial fibrillation occurs predominantly in elderly persons and is frequently associated with underlying cardiac diseases. In 15% to 30% of patients, however, an etiology is absent (i.e., lone AF) (16,17). Although AF has been regarded a sporadic and acquired disease, the familial aggregation of AF has been shown to be more frequent than previously recognized (18,19). Chen et al. (7) found the first gene mutation responsible for familial AF in *KCNQ1*, which encodes the α-subunit of slow delayed rectifier potassium (K^+) channels. Since then, 3 additional genes—all of which encode cardiac K^+ channels—responsible for familial AF have been identified: *KCNE2* (8), *KCNJ2* (9), and *KCNA5* (10). Recently, loss-of-function *SCN5A* mutations (D1275N) were reported to be associated with 2 families who have atrial arrhythmias (AF, cardiac conduction disease, and sick sinus syndrome) with dilated cardiomyopathy (11,12). More recently, an *SCN5A* mutation (N1986K) was identified in a family with lone AF (13). Functional assays on the N1986K channels revealed a hyperpolarized shift of steady-state inactivation, indicating a loss-of-function type modulation. One of the affected members underwent pacemaker implantation due to sick sinus syndrome, suggesting the underlying conduction disturbance resulting from the Na^+ channel loss-of-function. In addition, a common polymorphism (H558R) in *SCN5A*, present in 20% of the population (20), reduces Na^+ current density (21). The screening for the polymorphism in 157 patients with lone AF revealed that the R558 allele was more common in patients with lone AF than in the control subjects and as such was considered to be a risk factor for lone AF (22). However, none of the M1875T-positive individuals carried the R558 allele.

These reports implicate a potential relationship between decreased Na^+ currents and AF; however, to date, an *SCN5A* gain-of-function mutation has never been linked to AF.

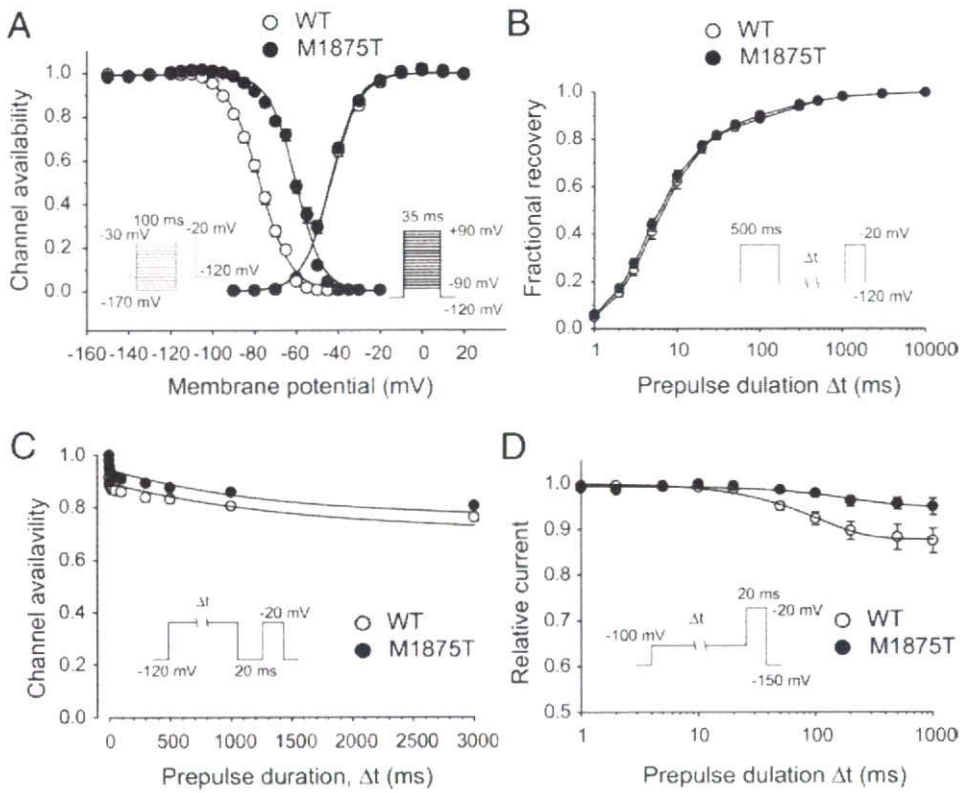

Figure 5 **Gating Properties for M1875T Channels**

Detailed parameters are given in Table 2. **(A)** Voltage dependence of relative sodium (Na^+) conductance activation and steady-state inactivation were determined by means of the voltage protocols, as shown in the inset. Curves were fit with the Boltzmann equation, $I/I_{max} = (1 + \exp[V-V_{1/2}]/k)^{-1}$ to determine the membrane potential for half-maximal inactivation or activation ($V_{1/2}$) and the slope factor k. Note that M1875T channels showed a pronounced depolarized shift (+16.4 mV) in the $V_{1/2}$ of steady-state inactivation compared with wild-type (WT). **(B)** Time course of recovery from inactivation was elicited with a double pulse protocol. Data were fit with a 2 exponential equation: $I/I_{max} = A_f \times (1 - \exp[-t/\tau_f]) + A_s \times (1 - \exp[-t/\tau_s])$, where A_f and A_s are fractions of fast and slow inactivation components, and τ_f and τ_s are the time constants of fast and slow inactivation components, respectively. **(C)** Onset of slow inactivation. Time course of entry into the slow inactivation state was obtained by a double pulse protocol. Curves were fit with a single exponential equation: $I/I_{max} = y0 + A \times \exp(-t/\tau)$. **(D)** Closed-state inactivation. The transfer rate of Na^+ channels from closed-state to inactivated closed-state without an intervening opening state was measured by a double pulse protocol. Time course for development of closed-state inactivation was fit with a single exponential equation: $I/I_{max} = y0 + A \times \exp(-t/\tau)$. The extent of closed-state inactivation was significantly less and the time constant larger in M1875T channels in comparison with WT.

Unique gain-of-function properties of M1875T Na^+ channels. To date, *SCN5A* gain-of-function mutations have been reportedly linked to only 1 phenotype, LQTS3. Persistent inward Na^+ currents observed in these mutant channels are considered to cause QT prolongation. However, M1875T channels did not display persistent inward Na^+ currents (Fig. 4E). This might explain why all of the affected and mutation-positive individuals in our study exhibited normal QT interval, with the exception of 1 individual who received disopyramide therapy. The functional properties of M1875T Na^+ channels were quite distinct from those of LQTS3. The most prominent change was a +16.4 mV shift in the steady-state inactivation. This is, to the best of our knowledge, the greatest depolarization shift in all of the previously reported SCN5A mutants. Some of the LQTS3 mutants (E1295K, A1330P, A1330T, and I1768V) showed a similar depolarizing shift of the steady-state inactivation without persistent inward Na^+ currents; however, the extent of the depolarizing shift was much less than M1875T (all were $<+10$ mV). The M1875T channels displayed the increased peak Na^+ current density (Fig. 4D), perhaps due to the large depolarized shift in steady-state inactivation. Interestingly, the location of the mutation is within a complex region that includes Ca^{2+} binding EF-hand like motifs and a putative binding site for calmodulin (23), and thus the mutation might disrupt inactivation by altered calcium sensitivity.

The potential mechanisms by which the identified gain-of-function mutation might lead to PAC or AF could be explained as the following: first, increased inward Na^+ currents might cause repolarization failure or early afterdepolarizations, thereby inducing triggered activities; and second, the increased Na^+ currents might increase the conduction velocity and facilitate the maintenance of the fibrillation wave. However, further studies are needed to elucidate the underlying mechanisms.

Genotype–phenotype relationship and clinical implications. Quite impressively, the affected family members shared a similar clinical course with high penetrance—frequent PACs and ATs first appeared during their teens and subsequently progressed to AF (Fig. 1A). Increased automaticity and irritability in the atrium was demonstrated by recurrent atrial arrhythmias that were resistant to ablation or drug therapy, induced PACs during exercise (Fig. 1C), and numerous ectopic firings and increased excitability throughout the right atrium during catheter ablation (Fig. 2). Because Na^+ channels encoded by *SCN5A* are expressed in both the atrium and ventricle, it remains unknown why our patients showed only atrial arrhythmias but not ventricular arrhythmias. The different electrophysiological properties between atrial and ventricular cells might be the underlying cause. Resting membrane potential is more depolarized, and the peak Na^+ current density is larger in atrial cells than in ventricular cells in dogs (24). The critical depolarization and current threshold for action potential initiation are smaller in atrial cells than in ventricular cells, indicating that atrial cells are more readily excitable than ventricular cells (25).

Conclusions

We identified a novel *SCN5A* gain-of-function mutation that causes a familial form of AF without any underlying structural heart diseases, which provides us with new insight into the pathogenesis of the commonly occurring form of AF.

Acknowledgment

The authors thank Richard Kaszynski for his critical reading of the manuscript.

Reprint requests and correspondence: Dr. Masaharu Akao, Department of Cardiovascular Medicine, Kyoto University Graduate School of Medicine, 54 Shogoin Kawahara-cho, Sakyo-ku, Kyoto, 606-8507, Japan. E-mail: akao@kuhp.kyoto-u.ac.jp.

REFERENCES

1. Chen Q, Kirsch GE, Zhang D, et al. Genetic basis and molecular mechanism for idiopathic ventricular fibrillation. Nature 1998;392:293–6.
2. Akai J, Makita N, Sakurada H, et al. A novel SCN5A mutation associated with idiopathic ventricular fibrillation without typical ECG findings of Brugada syndrome. FEBS Lett 2000;479:29–34.
3. Schott JJ, Alshinawi C, Kyndt F, et al. Cardiac conduction defects associate with mutations in SCN5A. Nat Genet 1999;23:20–1.
4. Benson DW, Wang DW, Dyment M, et al. Congenital sick sinus syndrome caused by recessive mutations in the cardiac sodium channel gene (SCN5A). J Clin Invest 2003;112:1019–28.
5. Wang Q, Shen J, Splawski I, et al. SCN5A mutations associated with an inherited cardiac arrhythmia, long QT syndrome. Cell 1995;80:805–11.
6. Makiyama T, Akao M, Tsuji K, et al. High risk for bradyarrhythmic complications in patients with Brugada syndrome caused by SCN5A gene mutations. J Am Coll Cardiol 2005;46:2100–6.
7. Chen YH, Xu SJ, Bendahhou S, et al. KCNQ1 gain-of-function mutation in familial atrial fibrillation. Science 2003;299:251–4.
8. Yang Y, Xia M, Jin Q, et al. Identification of a KCNE2 gain-of-function mutation in patients with familial atrial fibrillation. Am J Hum Genet 2004;75:899–905.
9. Xia M, Jin Q, Bendahhou S, et al. A Kir2.1 gain-of-function mutation underlies familial atrial fibrillation. Biochem Biophys Res Commun 2005;332:1012–9.
10. Olson TM, Alekseev AE, Liu XK, et al. Kv1.5 channelopathy due to KCNA5 loss-of-function mutation causes human atrial fibrillation. Hum Mol Genet 2006;15:2185–91.
11. McNair WP, Ku L, Taylor MRG, et al. SCN5A mutation associated with dilated cardiomyopathy, conduction disorder, and arrhythmia. Circulation 2004;110:2163–7.
12. Olson TM, Michels VV, Ballew JD, et al. Sodium channel mutations and susceptibility to heart failure and atrial fibrillation. JAMA 2005;293:447–54.
13. Ellinor PT, Nam EG, Shea MA, Milan DJ, Ruskin JN, Macrae CA. Cardiac sodium channel mutation in atrial fibrillation. Heart Rhythm 2008;5:99–105.
14. Shirai N, Makita N, Sasaki K, et al. A mutant cardiac sodium channel with multiple biophysical defects associated with overlapping clinical features of Brugada syndrome and cardiac conduction disease. Cardiovasc Res 2002;53:348–54.
15. Bordachar P, Reuter S, Garrigue S, et al. Incidence, clinical implications and prognosis of atrial arrhythmias in brugada syndrome. Eur Heart J 2004;25:879–84.
16. Murgatroyd FD, Camm AJ. Atrial arrhythmias. Lancet 1993;341:1317–22.
17. Levy S, Maarek M, Coumel P, et al. Characterization of different subsets of atrial fibrillation in general practice in France: the ALFA study. Circulation 1999;99:3028–35.
18. Darbar D, Herron KJ, Ballew JD, et al. Familial atrial fibrillation is a genetically heterogeneous disorder. J Am Coll Cardiol 2003;41:2185–92.
19. Ellinor PT, Yoerger DM, Ruskin JN, MacRae CA. Familial aggregation in lone atrial fibrillation. Hum Genet 2005;118:179–84.
20. Ackerman MJ, Splawski I, Makielski JC, et al. Spectrum and prevalence of cardiac sodium channel variants among black, white, Asian, and Hispanic individuals: implications for arrhythmogenic susceptibility and Brugada/long QT syndrome genetic testing. Heart Rhythm 2004;1:600–7.
21. Makielski JC, Ye B, Valdivia CR, et al. A ubiquitous splice variant and a common polymorphism affect heterologous expression of recombinant human SCN5A heart sodium channels. Circ Res 2003;93:821–8.
22. Chen LY, Ballew JD, Herron KJ, Rodeheffer RJ, Olson TM. A common polymorphism in SCN5A is associated with lone atrial fibrillation. Clin Pharmacol Ther 2007;81:35–41.
23. Deschenes I, Neyroud N, DiSilvestre D, Marban E, Yue DT, Tomaselli GF. Isoform-specific modulation of voltage-gated Na(+) channels by calmodulin. Circ Res 2002;90:E49–57.
24. Burashnikov A, Di Diego JM, Zygmunt AC, Belardinelli L, Antzelevitch C. Atrium-selective sodium channel block as a strategy for suppression of atrial fibrillation: differences in sodium channel inactivation between atria and ventricles and the role of ranolazine. Circulation 2007;116:1449–57.
25. Golod DA, Kumar R, Joyner RW. Determinants of action potential initiation in isolated rabbit atrial and ventricular myocytes. Am J Physiol Heart Circ Physiol 1998;274:H1902–13.

Key Words: arrhythmia ▪ atrial fibrillation ▪ genetics ▪ ion channels ▪ sodium.

European Journal of Pharmacology 600 (2008) 18–25

Contents lists available at ScienceDirect

European Journal of Pharmacology

journal homepage: www.elsevier.com/locate/ejphar

Molecular and Cellular Pharmacology

Cinnamyl-3,4-dihydroxy-α-cyanocinnamate and nordihydroguaiaretic acid inhibit human Kv1.5 currents independently of lipoxygenase

Ying-Zi Gong [a,b,c], Wei-Guang Ding [a,*], Jie Wu [d], Keiko Tsuji [b], Minoru Horie [b], Hiroshi Matsuura [a]

[a] Department of Physiology, Shiga University of Medical Science, Otsu, Shiga 520-2192, Japan
[b] Department of Cardiovascular and Respiratory Medicine, Shiga University of Medical Science, Otsu, Shiga 520-2192, Japan
[c] Department of Cardiovascular Medicine, Fourth Affiliated Hospital Harbin University, Harbin, 150001, China
[d] Pharmacology Department, Medical School of Xi'an Jiaotong University, Xi'an Shaanxi 710061, China

ARTICLE INFO

Article history:
Received 26 April 2008
Received in revised form 15 September 2008
Accepted 5 October 2008
Available online 10 October 2008

Keywords:
Kv1.5
I_{Kur}
CDC
NDGA
Lipoxygenase
Open channel block
Site-directed mutagenesis

ABSTRACT

In humans, Kv1.5 (hKv1.5) channels conduct the ultra-rapid delayed rectifier K^+ current (I_{Kur}) that is important for the repolarization of cardiac action potentials. We aimed at examining the effect of lipoxygenase inhibitors cinnamyl-3,4-dihydroxy-α-cyanocinnamate (CDC), nordihydroguaiaretic acid (NDGA), and gossypol on hKv1.5 wild-type and mutant channels heterologously expressed in Chinese hamster ovary (CHO) cells, by use of the site-directed mutagenesis and whole-cell patch-clamp method. CDC and NDGA, but not gossypol, a structurally dissimilar inhibitor, reversibly inhibited hKv1.5 current in a concentration-dependent manner with IC_{50} of 5.7 μM and 16.4 μM, respectively. The blockade evoked by both drugs was voltage-dependent between −20 and +10 mV (voltage range of channel opening). Moreover, this blocking action was found to progress with time during depolarizing voltage steps with a more rapid block at higher concentrations. CDC induced slight but significant delay of the deactivation rate. However, NDGA markedly slowed the deactivation time course, resulting in a tail crossover phenomenon. The recovery time constants from current block at repolarizing potentials for CDC and NDGA were 60.9 ms and 129.7 ms, respectively. Mutation of arginine 487 to valine (R487V) in the outer pore region of the channel significantly reduced the CDC action. These results demonstrate for the first time that CDC and NDGA block hKv1.5 channels by binding to the open state of the channels, independently of their effects on lipoxygenase activity. The putative binding site for CDC appears to be related to arginine 487 located in the outer pore region.

1. Introduction

In the cardiac cells, many voltage-gated K^+ (Kv) channels including the transient outward current (I_{to}) and the three (ultra-rapid, rapid, and slow) delayed rectifier potassium currents (I_{Kur}, I_{Kr}, and I_{Ks}, respectively) play an important role in determining the action potential duration. Therefore, these voltage-dependent potassium channels could be potent targets for the action of antiarrhythmic drugs (Knobloch et al., 2002). It is well known that atrial fibrillation is the most frequent cardiac arrhythmia and is associated with significant morbidity and mortality (Chugh et al., 2001). However, the available drugs for the treatment of atrial fibrillation often cause unwanted adverse effects such as the occasional generation of ventricular arrhythmias evoked by excess prolongation of action potential duration (Bril, 2002; Roden, 2001). Because I_{Kur} is expressed in atrial but scarcely in ventricular cells in humans (Li et al., 1996; Stump et al., 2005), I_{Kur} may therefore provide an attractive molecular target for treatment of atrial fibrillation. The molecular component that underlies cardiac I_{Kur} is the Kv1.5 channel (Fedida et al., 1993; Wang et al., 1993b). A line of experiments have been made to identify novel blockers of Kv1.5 (Brendel and Peukert, 2003; Trotter et al., 2006; Varro et al., 2004) and to study their binding site to the channel. Recent studies have shown that several residues that are located near the outer pore region, pore helix as well as in the transmembrane segments (S6) of the human Kv1.5 channels (hKv1.5) are important for the binding of these channel blockers (Decher et al., 2004, 2006; Herrera et al., 2005; Rezazadeh et al., 2006).

Cinnamyl-3,4-dihydroxy-α-cyanocinnamate (CDC) and nordihydroguaiaretic acid (NDGA), are common lipoxygenase inhibitors used in conjunction to study signaling related to biologically active arachidonic acid and its metabolites (Glitsch et al., 2002; Meves, 1994). Arachidonic acid is either intracellularly released or reaches the cell membrane via the circulation. Numerous studies have previously shown the effect of arachidonic acid on various types of ion channels, activating some and blocking others (Meves, 1994). Extracellularly applied arachidonic acid and other polyunsaturated fatty acids are reported to inhibit Kv1.5 channel markedly (Honore et al., 1994). The mechanism related to the arachidonic acid effects varies depending on the different types of ion channels. However, in some cases arachidonic

* Corresponding author. Department of Physiology, Shiga University of Medical Science, Seta Tsukinowa-cho Otsu, Shiga 520-2192, Japan. Tel.: +81 77 548 2152; fax: +81 77 548 2348.
E-mail address: ding@belle.shiga-med.ac.jp (W.-G. Ding).

0014-2999/$ - see front matter © 2008 Elsevier B.V. All rights reserved.
doi:10.1016/j.ejphar.2008.10.010

acid has direct actions on the ion channel or its lipid environment (Meves, 1994). It is reasonable to consider that CDC and NDGA are structurally close enough to these lipid molecules to affect either the activity of lipoxygenase or the channel activity in a similar manner. Indeed, these lipoxygenase inhibitors could share some actions on the ion channels unrelated to lipoxygenase inhibition. It has been reported that CDC can directly activate background K^+ channels (Danthi et al., 2004), and NDGA can directly enhance Ca^{2+}-dependent K^+ currents in isolated coronary arterial smooth muscle cells (Yamamura et al., 1999). In addition, NDGA was also reported to inhibit voltage-activated Ca^{2+} currents in pituitary cells (Korn and Horn, 1990), fibroblasts (Wang et al., 1993a) and voltage-sensitive K^+ currents in isolated type I carotid body cells (Hatton and Peers, 1997) independently of lipoxygenase inhibition. Therefore, the blocking mechanism or a binding site of the lipoxygenase inhibitors is an important issue with respect to the understanding of the reported fatty acids effects on cardiac function, diseased states and drug development perspective.

In light of these studies, we have investigated the effects of CDC and NDGA on hKv1.5 channels heterologously expressed in CHO cells by using the whole-cell patch-clamp technique. Our findings indicate that CDC or NDGA interacts with hKv1.5 channels in a lipoxygenase-independent manner and directly inhibits hKv1.5 currents as an open channel blocker. The R487 located in the outer pore region is demonstrated as a putative binding site for CDC.

2. Materials and methods

2.1. Cell culture and site-directed mutagenesis

Chinese hamster ovary (CHO) cells were maintained in Dulbecco's modified Eagle's medium/Ham's F-12 (DMEM/F-12) supplemented with 10% fetal bovine serum (GIBCO) and antibiotics (100 IU ml^{-1} penicillin, 100 μg ml^{-1} streptomycin) in an incubator gassed with 5% CO_2 and 95% air at 37 °C. Full-length cDNA of human hKv1.5 was ligated to the mammalian expression vector pcDNA3 (kindly provided by Dr. D. Fedida; University of British Columbia, Canada). Polymerase chain reaction based site-directed mutagenesis was applied to introduce mutations into hKv1.5 cDNA by using Quikchange Kit (Stratagene, La Jolla, CA, USA). All products were fully sequenced (ABI3100x/, Applied Biosystems, Foster City, CA) to ensure the fidelity of the PCR reactions. Wild type hKv1.5 cDNA and hKv1.5 mutants (T462C, H463C, T480A, R487V, A501V, I502A, I508A, L510A and V516A cDNA) were transiently transfected into CHO cells together with green fluorescent protein (GFP) cDNA (wild type or mutants 0.5 μg+GFP 0.5 μg) by using Lipofectamine (Life Technologies, Inc.). In addition, a KCNA5 synonymous polymorphism P532L (kindly provided by Dr. DM. Roden; Vanderbilt University School of Medicine, USA) was also tested. After transfection for 24–48 h, the GFP-positive cell was used for the patch-clamp study.

2.2. Patch-clamp recordings

Whole-cell membrane currents or macroscopic currents were recorded with an EPC-8 patch-clamp amplifier (HEKA, Lambrecht, Germany). Data were low-pass filtered at 1 kHz, acquired at 5 kHz through an LIH-1600 AD/DA interface (HEKA) using Pulse/PulseFit software (HEKA). Patch electrodes were fabricated from glass capillaries (Narishige, Japan) using a Sutter P-97 microelectrode puller (Sutter Instrument Co., USA) and had a resistance of 2.0–3.0 MΩ when filled with the pipette solution. A coverslip with adherent CHO cells was placed on the glass bottom of a recording chamber (0.5 ml in volume) and continuously perfused at a rate of 2 ml min^{-1} with bath solution at 25 °C. The hKv1.5 whole-cell membrane currents were elicited by applying 300-ms depolarizing steps from a holding potential of −80 mV to various levels. Recovery from inhibition at repolarizing potentials was measured by following a double-pulse protocol; the first pre-pulse of a 500-ms depolarizing potential of +40 mV from a holding potential of −80 mV was followed by a 50-ms test pulse of +40 mV after increasing time intervals between 10 and 2000 ms at −80 mV. Every cycle of the double pulse protocol was 30 s. The time course for recovery from block was determined by plotting the normalized peak current (test pulse/pre-pulse) as a function of various interpulse intervals. This time course was fitted with a single exponential function. As previously described (Lagrutta et al., 2006), the derived time constant (τ) for the kinetics of recovery from block in the closed state (repolarized membrane potentials) is related to the off kinetic rate by the expression $1/\tau = k_{off}$. In addition, the macroscopic currents were evoked by 500-ms depolarizing step from a holding potential of −80 mV to +50 mV, recorded from an inside-out membrane patch.

2.3. Solutions and chemicals

The bath solution for whole cell recording contained (in mM): 140 NaCl, 5.4 KCl, 1.8 $CaCl_2$, 0.5 $MgCl_2$, 0.33 NaH_2PO_4, 5.5 glucose and 5.0 HEPES (pH was adjusted to 7.4 with NaOH). Agents added to the bath solutions included CDC (BIOMOL), NDGA (Sigma) and gossypol (BIOMOL). These compounds were dissolved in dimethyl sulfoxide (DMSO) to make stock solution of 20–50 mM. The final concentration of DMSO used in the present experiments was less than 0.1%, which had no effect on hKv1.5 currents. The pipette solution contained (in mM): 70 potassium aspartate, 40 KCl, 10 KH_2PO_4, 1 $MgSO_4$, 3 Na_2-ATP (Sigma), 0.1 Li_2-GTP (Roche Diagnostics GmbH, Mannheim, Germany), 5 EGTA and 5 HEPES, and pH was adjusted to 7.2 with KOH. For inside-out patches, the electrodes were filled with the following solution (in mM): 130 NaCl, 5.0 KCl, 2.8 sodium acetate, 1.0 $MgCl_2$, pH 7.4 with NaOH. The external recording solution for inside-out patches contained (in mM): 120 potassium aspartate, 20 KCl, 4.0 Na_2ATP, 5.0 HEPES, 1.0 $MgCl_2$, pH 7.2 with KOH.

2.4. Data analysis

The concentration–response relationship for the current inhibition (y) by CDC or NDGA was fitted to the Hill equation:

$$y = E_{max}/(1 + (IC_{50}/[drug])^{n_H}) \quad (1)$$

where E_{max} is the maximum effect of block expressed as a percentage, IC_{50} is the concentration of CDC or NDGA causing a half-maximal inhibition, and n_H is the Hill coefficient. A first-order blocking scheme was used to describe the drug–channel interaction (Snyders and Yeola, 1995, Yeola et al., 1996). The apparent rate constants for binding (k_{+1}) and unbinding (k_{-1}) were obtained from the following equations:

$$\tau_D = 1/(k_{+1}[D] + k_{-1}) \quad (2a)$$

$$K_d = k_{+1}/k_{-1} \quad (2b)$$

where τ_D is the drug-induced time constant, which was calculated by single exponential fits to the current decay during depolarizing step to +30 mV. The apparent dissociation constant K_d is expressed as $K_d = k_{+1}/k_{-1}$. Data for voltage-dependence of hKv1.5 activation was fitted with a Boltzmann equation:

$$I_{tail} = 1/(1 + \exp((V_{1/2} - V_m)/k)) \quad (3)$$

where I_{tail} is the tail current amplitude normalized with reference to the maximum value measured at +50 mV, $V_{1/2}$ is the half-maximal voltage, V_m is the test potential and k is the slope factor. The deactivation kinetics was also determined by a single exponential fit of tail current trace.

2.5. Statistics

All data were expressed as mean ± S.E.M. Statistical comparisons between two groups were analyzed using Student's *t* test. Comparisons among multiple groups were analyzed using ANOVA, followed by Dunnett' post hoc test and differences were considered significant at $P<0.05$.

3. Results

3.1. Inhibitory action of CDC on hKv1.5 current

Fig. 1A shows superimposed current traces evoked by 300-ms depolarizing voltage-clamp steps pulses applied from a holding potential of −80 mV to various test potentials (−50 to +50 mV) in 10-mV steps under control conditions (left-hand panel) and 5 min after exposure to 5 μM CDC (right-hand panel). Outward currents were followed by decaying outward tail currents upon repolarization to the −40 mV. Under control conditions, the depolarizing pulses to potentials ≥−30 mV elicited an activating outward current which progressively increased with further depolarizing pulses. Moreover, hKv1.5 current activated rapidly upon depolarization to reach a peak and then remained stable during moderate depolarizing test steps (≤+30 mV). However, the current inactivated minimally during more depolarized test potentials (≥+40 mV), as is consistent with previous reports (Choi et al., 2000; Herrera et al., 2005; Rezazadeh et al., 2006). The activation time constant of 1.68 ± 0.1 ms ($n=6$) was obtained by fitting a single exponential function to the current traces during the initial 30 ms of depolarizing step to +30 mV.

Bath application of 5 μM CDC did not significantly alter the activation time constant (1.51 ± 0.86 ms at +30 mV; $n=6$, $P>0.05$), but only slightly decreased the peak amplitude of hKv1.5 current. On the other hand, CDC produced a time-dependent decline in outward currents during depolarizing pulses, which was more marked at stronger positive potentials. Fig. 1B shows the resulting current-voltage (*I–V*) relationships for these data constructed by plotting the current amplitudes at the end of 300-ms depolarizations as a function of the test pulse voltage, suggesting that CDC-induced current block was over the whole potential range for activation. The voltage dependence of activation of hKv1.5 current in the absence or presence of CDC was calculated by fitting a Boltzmann Eq. (3) to the amplitude of tail currents recorded at −40 mV following depolarizing steps (Fig. 1C). As shown in Fig. 1C, the drug significantly shifted the voltage dependence of channel opening to more hyperpolarized potentials, as described for the action of other drugs (Perchenet and Clement-Chomienne, 2000; Choe et al., 2003). In a total of seven cells, $V_{1/2}$ averaged −10.0 ± 1.9 mV in control and −21.6 ± 2.0 mV ($P<0.01$) in the presence of CDC, while k was 9.7 ± 1.1 mV in control and 7.2 ± 1.1 mV ($P<0.05$) in the presence of the drug.

To quantify this voltage dependence of hKv1.5 inhibition, the relative current ($I_{CDC}/I_{Control}$) was plotted as a function of membrane potentials (Fig. 1D). The hKv1.5 channel was activated with a threshold potential of −40 mV and the channel conductance peak was attained near to +20 mV. The blocking action of CDC on the current was voltage-dependent with a higher degree of inhibition between −20 and +10 mV that is the voltage range for channel opening. However, at potentials positive to +10 mV where the full opening of channels is developed, current reduction exhibited shallower voltage dependence. Taken together, these data suggest that CDC-induced blocking of hKv1.5 current develops mainly after channel opening. We next examined the open state binding of CDC by analyzing the tail current, which reflecting the process from the opening to the close state of the channels. Fig. 1E shows the deactivation time constants measured by fitting a single exponential function to the outward tail current at

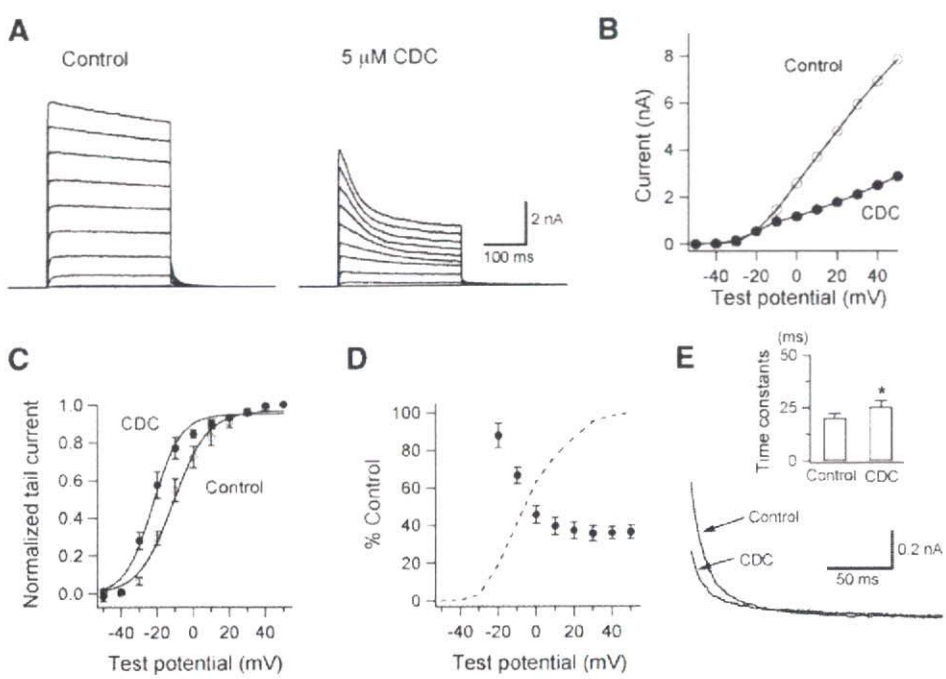

Fig. 1. Inhibitory action of CDC on hKv1.5 channels heterologously expressed in a CHO cell. A: Superimposed hKv1.5 channel currents elicited during 300-ms depolarizing steps from a holding potential of −80 mV to potentials between −50 and +50 mV in 10-mV increments, followed by a repolarization step to −40 mV, before (Control) and 5 min after exposure to 5 μM CDC. B: *I–V* relationships obtained from the records in panel A for late currents measured at the end of test steps in control (open circles) and during exposure to 5 μM CDC (filled circles). C: *I–V* relationships for normalized tail currents in control and during exposure to 5 μM CDC. The smooth curves through the data points were fit with a Boltzmann equation. D: Late current amplitude in the presence of CDC is plotted as a percentage of control amplitude in the absence of the drug (% Control). Data points represent means ± S.E.M. of six different cells. The dashed curve represents the activation curve obtained in control conditions (see Fig. 1C). E: Tail currents were recorded at −40 mV after step to +50 mV from a holding potential of −80 mV for 300-ms in control and during exposure to 5 μM CDC. The decay in tail currents were fitted to a single exponential function. The inset shows summary data of time course of deactivation in control and presence of CDC.

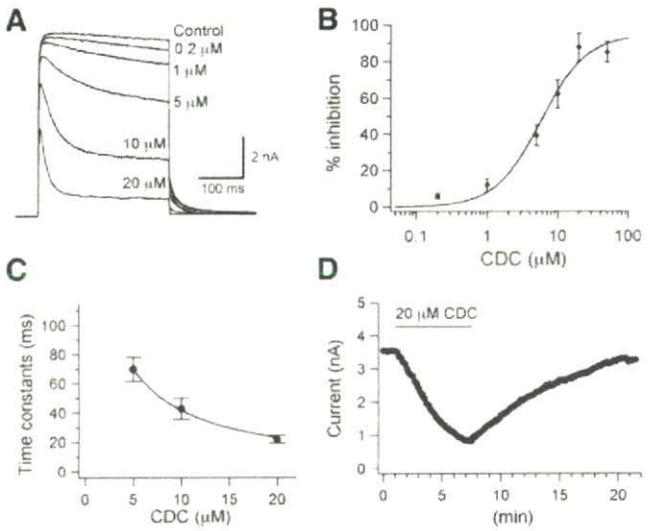

Fig. 2. Concentration-dependent and reversible block of hKv1.5 current by CDC. A: Superimposed hKv1.5 current traces evoked by 300-ms depolarizing step from a holding potential of −80 mV to +30 mV, before (Control) and during exposure to various concentrations (0.2, 1, 5, 10, and 20 μM) of CDC. B: Concentration–response relationship for the inhibition of hKv1.5 current by CDC. Percentage inhibition (% inhibition) represents the fraction of hKv1.5 current reduced by each concentration of CDC with reference to the control amplitude, measured at the end of 300-ms depolarizing step to +30 mV. The smooth curve through the data points represents a least-squares fit of a Hill equation. The IC_{50} value for CDC was 5.7 μM. C: The drug-induced time constant at +30 mV was obtained from single exponential fits to the decay phase of the current traces and plotted as a function of the drug concentration (5, 10, and 20 μM). The solid line represents the fit of the data to the hyperbolic function (see text). D: The cell was repetitively depolarized every 10 s from a holding potential of −80 mV to +30 mV for 300-ms. The amplitude of outward currents measured at the end of depolarizing pulse was plotted as a function of time for the entire experiment. CDC (20 μM) was added to the bath during the period indicated by the horizontal bar.

−40 mV before and during exposure to CDC, respectively. The values for time constant in the absence and presence of CDC were 20.1 ± 2.3 ms and 25.5 ± 2.8 ms ($n = 10$; $P < 0.05$, Student's paired t test) thus, indicating that the deactivation process is slightly but significantly slowed by the drug.

3.2. Concentration-dependent and reversible inhibition of hKv1.5 by CDC

Fig. 2A shows representative hKv1.5 current recordings under control conditions and in the presence of CDC at various concentrations between 0.2 and 20 μM. The current was evoked every 10 s by 300-ms depolarizing voltage steps to +30 mV from a holding potential of −80 mV, before and during exposure to increasing concentrations of CDC in a cumulative manner. CDC induced-reduction was most potent in the late current level at the end of the 300-ms depolarizing pulses, at any given concentration, suggesting that CDC induced a gradual development of channel inhibition during the open state of the channel. Fig. 2B shows the concentration-dependent inhibition of the hKv1.5 current by CDC measured at the end of depolarizing step to +30 mV. The plots of late current as a function of CDC concentration were fitted to the Hill Eq. (1), and the calculated IC_{50} and n_H were 5.7 μM and 1.3, respectively ($n = 6$).

As shown in Fig. 2C, CDC elicited a concentration-dependent facilitation in the rate of current decay during the depolarizing step (to +30 mV). The decay of current trace in the presence of each concentration of CDC (5, 10, and 20 μM) was fitted to a single exponential function, which yielded a time constant (τ_D) for hKv1.5 current block. The time constant values obtained at low concentrations (0.2 and 1 μM) were omitted, because their current decay was too small to obtain correct fits. Plotting τ_D at +30 mV against each concentration and fitting it to a hyperbolic equation Eq. (2a), yielded binding (k_{-1}) and unbinding rate constants (k_{-1}) of 1.9 $\mu M^{-1}\ s^{-1}$ and 4.7 s^{-1}. From these values, an apparent K_d (2b) can be calculated to be

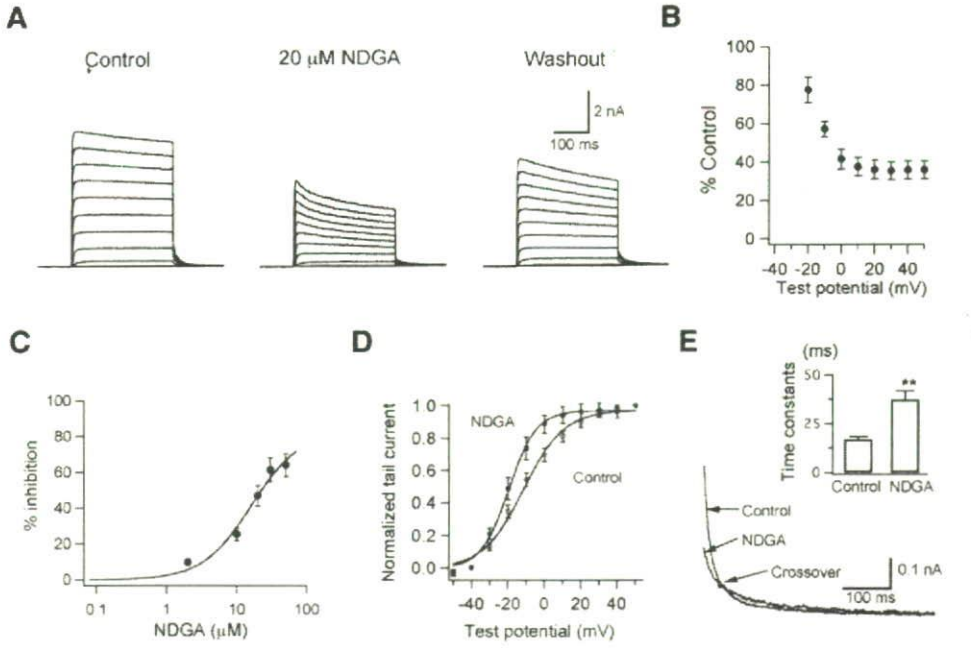

Fig. 3. Inhibitory action of NDGA on hKv1.5 channels. A: Superimposed hKv1.5 channel currents elicited during 300-ms depolarizing steps from a holding potential of −80 mV to potentials between −50 and +50 mV in 10-mV increments, followed by a repolarization step to −40 mV, before (Control) and 5 min after exposure to 20 μM NDGA. B: Late current amplitude in the presence of NDGA is plotted as a percentage of control amplitude in the absence of the drug (% Control). Data points represent means ± S.E.M. of five different cells. C: Concentration–response relationship for NDGA block. The smooth curve through the data points represents a least-squares fit of a Hill equation. The IC_{50} value for NDGA was 16.4 μM. D: I–V relationships for normalized tail currents in control (open circles) and during exposure to 20 μM NDGA (filled circles). The smooth curves through the data points were fit with a Boltzmann equation. E: Tail currents were recorded at −40 mV after step to +50 mV from a holding potential of −80 mV for 300-ms in control and during exposure to 20 μM NDGA. The inset shows summary data of time course of deactivation in control and presence of NDGA.

2.5 μM. This derived K_d is considerably close to the IC_{50} of 5.7 μM obtained from the concentration–response curve (Fig. 2B), suggesting that the inhibition of the hKv1.5 channel by CDC may follow a simple one-to-one reaction.

To investigate the reversibility of CDC effects on hKv1.5, a maximally effective concentration (20 μM) of CDC was applied. Fig. 2D shows the time course of changes in the current amplitude at the end of depolarizing pulse to +30 mV during exposure to CDC. The inhibition induced by CDC appeared within 20 s after drug being applied and reached the maximum degree of the inhibition within 5 min. The blocking effect of CDC was almost fully reversed following perfusion with drug-free bath solution (restored to 89.6±3.7% of its initial control value).

3.3. Inhibitory action of NDGA on hKv1.5 current

We next investigated the action of NDGA, which is another well-known lipoxygenase inhibitor. As summarized in Fig. 3, the action induced by NDGA on hKv1.5 current was fundamentally similar to that evoked by CDC. NDGA-induced block was also voltage- and concentration-dependent (with an IC_{50} of 16.4±1.3 μM) and reversible (Fig. 3A–C). After 8–10 min washout, the blocking effect of NDGA was markedly reversed (restored to 68.8±2.9% of its initial control value). The drug however, elicited a weaker time-dependent decline in the outward currents during depolarizing potentials (Fig. 1A), suggesting that NDGA is a weaker open channel blocker. Comparable to CDC, NDGA also did not significantly affect the activation time constant (1.63±0.94 ms at +30 mV, n=6, P>0.05 compared to control), but shifted the voltage dependence of channel opening to more hyperpolarized potentials (Fig. 3D, $V_{1/2}$ under control was −11.3 mV±2.2 mV; in the presence of NDGA was −19.5±1.8 mV, n=6, P<0.05).

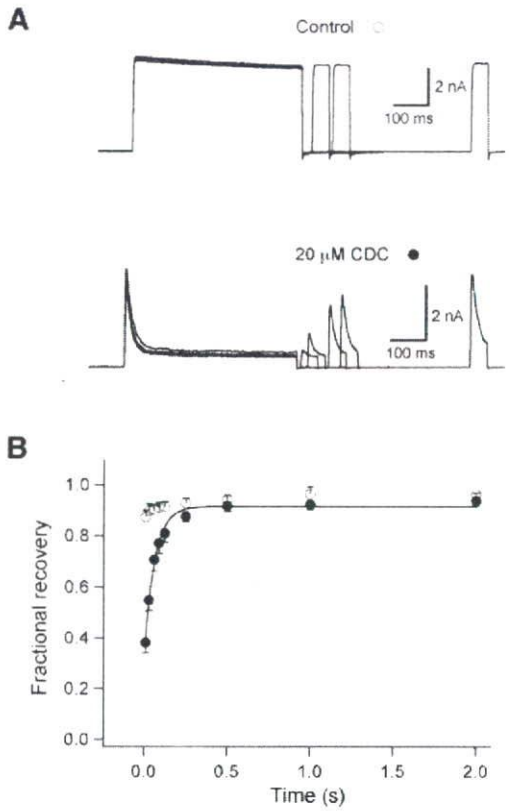

Fig. 4. Effect of CDC on the kinetics of hKv1.5 recovery from block. A: The degree of recovery from block at repolarizing potentials was measured by following a double-pulse protocol: the first pre-pulse of a 500-ms depolarizing potential of +40 mV from a holding potential of −80 mV was followed by a 50-ms test pulse of +40 mV after increasing time intervals between at −80 mV in the absence (control) and presence of 20 μM CDC. Every cycle of the double pulse protocol was 30 s. B: In the absence of the compound (open circles), the ratios of peak current (test pulse/pre-pulse) are close to 1 for all interpulse interval. In the presence of CDC (filled circles), the recovery from current inhibition upon repolarization was well fitted with a single exponential function, which yielded recovery time constant (τ) of 60.9 ms.

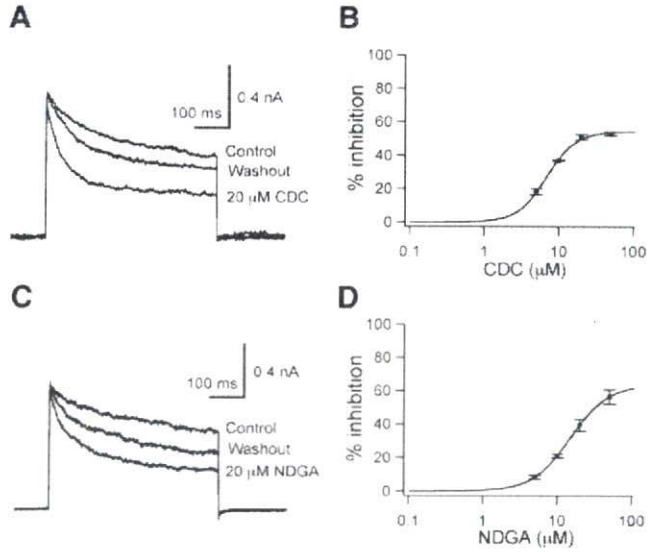

Fig. 5. Effects of CDC and NDGA on hKv1.5 current recorded from an inside-out membrane patch. A: Superimposed hKv1.5 current traces evoked by 500-ms depolarizing step from a holding potential of −80 mV to +50 mV, before (Control), during exposure to 20 μM CDC and after washout. B: Concentration–response relationship for the inhibition of hKv1.5 by CDC recorded from inside-out patches. Percentage inhibition (% inhibition) represents the fraction of hKv1.5 current reduced by each concentration of CDC with reference to the control amplitude, measured at the end of 500-ms depolarizing step. The IC_{50} value for CDC was 6.9 μM. C: Protocol is the same as in A. Note hKv1.5 currents before (Control), during exposure to 20 μM NDGA and after washout. D: Concentration–response relationship for the inhibition of hKv1.5 by NDGA recorded from inside-out patches. The IC_{50} value for NDGA was 15.1 μM.

However, in the presence of 20 μM NDGA, the decay of the tail current reflecting channel deactivation was markedly decelerated (Fig. 3E, control, 17.3±0.5 ms; NDGA, 33.9±3.9 ms, n=7, P<0.05), which resulted in a tail crossover phenomenon. The result suggests that the drug can induce a block of the available open channels at −40 mV, and its unbinding process was necessary before channels could close.

3.4. Effects of CDC and NDGA on the kinetics of hKv1.5 recovery from block

To further observe the properties of channel deactivation in detail, the recovery from inhibition at repolarizing potentials was measured by following a double-pulse protocol. Fig. 4A shows a typical example of the recovery kinetics from block of hKv1.5 channels at repolarizing potentials. In the absence of the compound (control), the ratios of peak current (test pulse/pre-pulse) were close to 1 for all interpulse. In the presence of CDC, the recovery from current inhibition upon repolarization was well fitted with a single exponential function, which yielded recovery time constant (τ) of 60.9 ms (Fig. 4B). As previously reported (Lagrutta et al., 2006), the derived τ for the kinetics of recovery from block in the closed state is related to the off kinetic rate by the expression $1/\tau = k_{off}$. Therefore, the value of k_{off} was 16.4 s^{-1}. This result suggests that more than 200 ms is required for the unbinding process of CDC from the channels, although the rate for CDC unbinding is rapid than that of reported diphenyl phosphine oxide (DPO) compounds (Lagrutta et al., 2006) and bisindolylmaleimide (Choi et al., 2000). The recovery from NDGA-induced inhibition at repolarizing potentials was measured by the same double-pulse protocol. In the presence of NDGA, the recovery from current inhibition was also well fitted with a single exponential function,

which yielded τ of 129.7 ms. The value of k_{off} for NDGA was 7.7 s^{-1}, suggesting that dissociation rate of NDGA from the channel at repolarizing potential is slower than that observed in CDC.

3.5. Effects of CDC and NDGA on hKv1.5 current recorded by the inside-out membrane patch

The characteristics of block by CDC and NDGA were studied in more detail in excised inside-out membrane patches from CHO cells expressing hKv1.5 currents (Fig. 5). Under these conditions, both CDC (Fig. 5A) and NDGA (Fig. 5C) at a concentration of 20 μM, produced significant inhibition of hKv1.5 currents (50.9±1.6% inhibition, $n=5$ for CDC; 39.4±3.6% inhibition, $n=4$ for NDGA). The concentration-dependent inhibition of the hKv1.5 current by CDC or NDGA measured at the end of depolarizing step to +50 mV were shown in Fig. 5B and D. The plots of current as a function of CDC concentration were fitted to the Hill equation and the calculated IC_{50} for CDC or NDGA were 6.9 μM and 15.1 μM. Thus, IC_{50} values for CDC or NDGA were in a similar range under both inside-out membrane patch and whole-cell conditions. However, the maximum block of CDC in inside-out patch was found to be smaller than that observed in whole-cell patch (87.7±7.7% inhibition by 20 μM CDC).

3.6. Direct block of CDC on hKv1.5

It was shown that the effects of CDC (Danthi et al., 2004) and NDGA (Yamamura et al., 1999; Korn and Horn, 1990; Wang et al., 1993a) on ion channels are independent of lipoxygenase activity. We tested whether the inhibition of hKv1.5 by CDC is mediated through lipoxygenase inhibition by applying gossypol, another pharmacological inhibitor of lipoxygenase with a markedly distinct structure (Glitsch et al., 2002). Fig. 6A shows the time-course of changes in the amplitude of hKv1.5 current measured at the end of depolarizing step to +30 mV during exposure to gossypol (10 μM) that is more than 20-fold greater than the IC_{50} for inhibition of lipoxygenase. Application of gossypol for 4-min did not elicit any inhibition of hKv1.5, however, continued exposure of 20 μM CDC immediately suppressed steady-state outward current by 84.7±2.1% ($n=5$), which was equal to the inhibition induced by CDC in the control condition (Fig. 6B). The inhibition of lipoxygenase was therefore not primarily involved in the CDC-induced reduction of the hKv1.5 current.

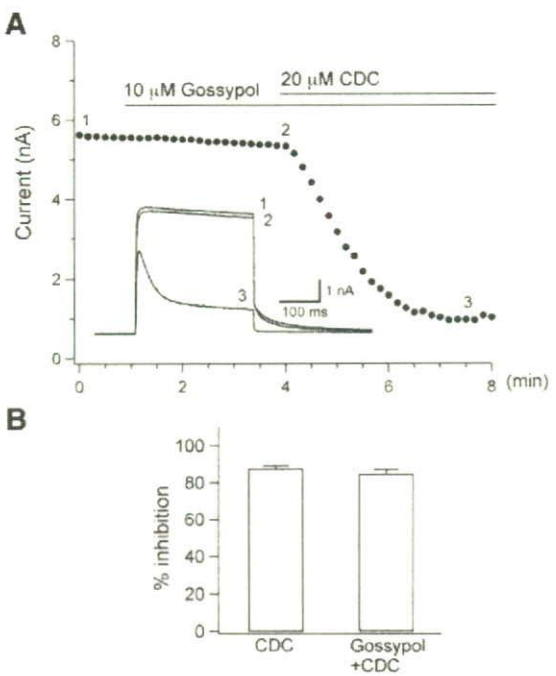

Fig. 6. Effect of gossypol on hKv1.5 current. A: The hKv1.5 current was repetitively activated with 300-ms depolarizing step to +30 mV from a holding potential of −80 mV and current amplitude measured at the end of depolarizing step was plotted. Inset shows the superimposed original current traces recorded at time points indicated by the numerals. B: Percentage block of the current by CDC measured at the end of depolarizing pulse to +30 mV under control condition and in the presence of gossypol.

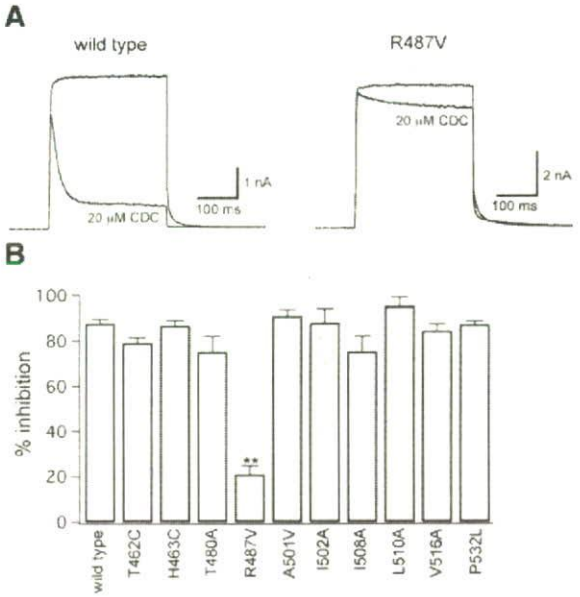

Fig. 7. Inhibitory action of CDC on hKv1.5 mutant channels. A: Representative current traces recorded from wild type and mutant channel (R487V) during 300-ms depolarizing step to +30 mV from a holding potential of −80 mV before and during exposure to 20 μM CDC. B: Percentage inhibition of wild type and various mutant channels of hKv1.5 by CDC (20 μM) was measured at the end of 300-ms depolarizing pulse. $^{**}P<0.01$ compared with wild type hKv1.5.

3.7. Inhibitory effects of CDC on mutant hKv1.5 channels

To examine the binding sites related to CDC action, nine residues located in the pore and S6 domain were mutated by site-directed mutagenesis based on the reported structural basis for the drug block (Decher et al., 2004, 2006; Herrera et al., 2005; Rezazadeh et al., 2006). The mutants used were T462C, H463C and R487V (located in the outer pore region), T480A (base of the pore helix), A501V, I502A, I508A, L510A, and V516A (S6 domain) and one polymorphism P532L located at the C-terminal. As previously reported, these mutant channels can produce the functional outward currents during depolarization (Decher et al., 2006; Rezazadeh et al., 2006; Simard et al., 2005). Fig. 7A indicates representative examples for the inhibitory effect of CDC (20 μM) on the wild type and R487V mutant channels activated during 300-ms depolarizing step to +30 mV from a holding potential of −80 mV. The kinetic properties between wild type and R487V mutant seemed to be qualitatively similar, however the inhibitory action induced by CDC was markedly decreased. Fig. 7B summarizes the CDC action on wild type and various mutant late currents measured at the end of depolarizing step to 30 mV, indicating that H462C, H463C, T480A, A501V, I502A, I508A, L510A, V516A and P532L mutant channels were inhibited by CDC to an extent similar to wild type channel. These results indicate that arginine 487 located in the outer pore region is important for CDC block on hKv1.5.

4. Discussion

The present study demonstrated that lipoxygenase inhibitors CDC and NDGA reversibly inhibited the hKv1.5 current in a concentration-, time-, and voltage-dependent manner. Lipoxygenase is one key

enzyme for production of biologically active arachidonic acid metabolites (Glitsch et al., 2002; Meves, 1994). It has been known that CDC exhibits more selective inhibition to 12-lipoxygenase (IC_{50}= 0.06 μM) than to 5-lipoxygenase (IC_{50}= 3.3 μM) and 15-lipoxygenase (IC_{50}= 1.9 μM; Cho et al., 1991). In addition, NDGA inhibits both 12- and 15 lipoxygenase enzymes with an IC_{50}-value of 26 μM and 1.0 μM, respectively (Beetens et al., 1986). In the present study, CDC and NDGA inhibited hKv1.5 current with an IC_{50} of 5.7 μM and 16.4 μM under whole-cell patch recording condition, respectively. It is thus likely that the potency of these compounds on the inhibition between hKv1.5 channel and lipoxygenase enzymes is comparatively similar. In addition, our data clearly demonstrate that the lipoxygenase pathways are not involved in the inhibitory action of CDC or NDGA on hKv1.5, because a structurally distinct lipoxygenase inhibitor gossypol did not produce any effect on the hKv1.5 (Fig. 6). A line of experiments has demonstrated that lipoxygenase inhibitors could modify several ionic channels unrelated to lipoxygenase inhibition. These channels included background K^+ channels (Danthi et al., 2004), Ca^{2+}-dependent K^+ channels (Yamamura et al., 1999), voltage-activated Ca^{2+} channels (Korn and Horn, 1990; Wang et al., 1993a) and voltage-sensitive K^+ channel (Hatton and Peers, 1997). The present study further confirmed this direct action of lipoxygenase inhibitors and demonstrated for the first time that CDC and NDGA reversely inhibited expressed hKv1.5 channel which is considered recently as an important molecular target for the treatment of atrial fibrillation.

In the previous studies, several drugs such as quinine, clofilium, and tetrapentylammonium (Snyders and Yeola, 1995), zatebradine (Valenzuela et al., 1996), bisindolylmaleimide (Choi et al., 2000), and mibefradil (Perchenet and Clement-Chomienne, 2000) have been documented to block Kv1.5 channels as an open channel blocker. Similar to these observations, CDC is also demonstrated to block hKv1.5 preferentially in the channel opening state, which is supported by the following evidences. Firstly, CDC-induced current decay was dependent on the depolarizing time and concentration of the drug (Fig. 2A and C). Second, CDC-evoked inhibition steeply increased at channel opening potentials between −20 and +10 mV (Fig. 1D). Third, CDC did not change the activation time course of the channel and only partially blocked the amplitude of peak current at the onset of depolarization (Figs. 1 and 2). NDGA shared some similar properties to the open channel blockers (Fig . 3A and B) although NDGA-induced current decay during the depolarizing step was weaker compared to that of CDC. In addition, compared to CDC, NDGA remarkably decreased the deactivation rate and resulted in a "crossover phenomenon" of tail current traces, which is consistent with the properties of other reported open channel blockers on Kv1.5 channels (Choi et al., 2000; Perchenet and Clement-Chomienne, 2000; Snyders and Yeola, 1995; Valenzuela et al., 1996). As demonstrated by our data (Fig. 4), in the presence of CDC, the recovery time constant from current inhibition is 60.9 ms, which is faster than that observed in NDGA (129.7 ms), suggesting that the dissociation rate of CDC from the channel during the repolarization process is rapid and thus it only slightly interferes the transitions of the channel from opening to closing.

The molecular basis of binding sites for hKv1.5 channel blockers have been previously studied (Decher et al., 2004, 2006; Herrera et al., 2005; Rezazadeh et al., 2006; Yeola et al., 1996). Amino acid substitutions in the midsection of S6 (T507 and V514) have been demonstrated to reduce the dissociation rate for quinidine, an antiarrhythmic drug (Yeola et al., 1996). In addition, local anesthetic drug benzocaine has been found to block hKv1.5 by interaction with T479 in the pore helix and T507, L510 and V514 in the S6 domain (Caballero et al., 2002). Moreover, the recently developed Kv1.5 blockers S0100176 and AVE0118 have also been proposed to bind to residues (T480, V505, I508, V512, and V516) that are predicted to face toward the central cavity of K^+ channels and to residues (I502 and L510) that are positioned away from the central cavity (Decher et al., 2004, 2006). Based on these previous suggestions, the present study tested the possible binding site in hKv1.5 for CDC by using mutant residues located in pore helix and S6 (T480A, A501V, I502A, I508A, L510A, and V516A) and other mutant residues located in the outer pore region (T462C, H463C and R487V). However, the present mutagenesis study has detected that only R487 is a putative binding site of CDC. This result is basically in agreement with the recent report that R487 is an only one key binding site for the inhibition of hKv1.5 by KN-93, a calcium/calmodulin-dependent protein kinase II inhibitor among the mutants in the outer pore region (Rezazadeh et al., 2006). T462, H463 and R487 are located in the outer pore region according to crystallized structure analysis of the Kv1.2 channel (Long et al., 2005), and R487 has position which is very close to the external mouth of the pore. R487 is the homolog position to T449 in *Shaker* (Jager and Grissmer, 2001). The position participates in the external tetraethylammonium (TEA)-binding site (Mackinnon and Yellen, 1990) and is also involved in regulating the C-type inactivation of Kv channels. For example, the substitution of R487 with valine markedly reduces the rate of C-type inactivation of hKv1.5 Na^+ currents (Wang et al., 2000). Failure of CDC blocking action on R487V mutant channel demonstrated by our study further supports these previous findings and suggests that R487 is an important residue in mediating the channel kinetics and determining the binding site for drugs.

It has been shown that positions 463 and 487 are crucial for the integrity of the external potassium binding site, possibly by electrostatic interaction (Jager and Grissmer, 2001). However, we could not conclude that the electrostatic interaction is related to the reduced sensitivity of mutant R487 channel to the compound because replacement of histidine (positive charged) to cysteine (neutral) at 463 had no effect on the potency of CDC binding. In addition, this reduced block was unlikely to be due to the hydrophilicity and hydrophobicity of residues tested in the present study. Indeed, the replacement of histidine to cysteine (hydropathy index changed from −3.2 to 2.5) at position 463 (Kyte and Doolittle, 1982) did not modify CDC-induced inhibition, whereas the replacement of arginine to valine (hydropathy index changed similarly from −4.5 to 4.2) at position 487 markedly reduced CDC effect.

In conclusion, the lipoxygenase inhibitors CDC and NDGA are open channel blockers that interact with hKv1.5 channels in a lipoxygenase-independent manner. The putative binding site for CDC is possibly related to R487 located in the outer of pore region. Because our results and previous data have clearly shown that CDC or NDGA can directly block many ionic channels, the experimenter should be careful when these inhibitors are used to study the ionic channel function. The present study may also provide some direction for the future development of effective and specific hKv1.5 channel blockers.

Acknowledgements

The authors thank Dr. D. Fedida and Dr. DM. Roden for the mammalian expressing vectors. This study was supported by Grant-in-aid for scientific Research (Nos.17590185 to H.M. and 19390212 to M.H.) from the Japan Society for the Promotion of Science.

References

Beetens, J.R., Loots, W., Somers, Y., Coene, M.C., Clerck, F.D.E., 1986. Ketoconazole inhibits the biosynthesis of leukotrienes in vitro and in vivo. Biochem. Pharmacol. 35, 883–891.

Brendel, J., Peukert, S., 2003. Blockers of the Kv1.5 channel for the treatment of atrial arrhythmias. Curr. Med. Chem. Cardiovasc. Hematol. Agents 1, 273–287.

Bril, A., 2002. Recent advances in arrhythmia therapy: treatment and prevention of atrial fibrillation. Curr. Opin. Pharmacol. 2, 154–159.

Caballero, R., Moreno, I., Gonzalez, T., Valenzuela, C., Tamargo, J., Delpon, E., 2002. Putative binding sites for benzocaine on a human cardiac cloned channel (Kv1.5). Cardiovasc. Res. 56, 104–117.

Cho, H., Ueda, M., Tamaoka, M., Hamaguchi, M., Aisaka, K., Kiso, Y., Inoue, T., Ogino, K., Tatsuoka, T., Ishihara, T., Noguchi, T., Morita, I., Murota, S., 1991. Novel caffeic acid derivatives: extremely potent inhibitors of 12-lipoxygenase. J. Med. Chem. 34, 1503–1505.

Choe, H., Lee, Y.K., Lee, Y.T., Choe, H., Ko, S.H., Joo, C.U., Kim, M.H., Kim, G.S., Eun, J.S., Kim, J.H., Chae, S.W., Kwak, Y.G., 2003. Papaverine blocks hKv1.5 channel current and human atrial ultrarapid delayed rectifier K^+ currents. J. Pharmacol. Exp. Ther. 304, 706–712.

Choi, B.H., Choi, J.S., Jeong, S.W., Hahn, S.J., Yoon, S.H., Jo, Y.H., Kim, M.S., 2000. Direct block by bisindolylmaleimide of rat Kv1.5 expressed in Chinese hamster ovary cells. J. Pharmacol. Exp. Ther. 293, 634–640.

Chugh, S.S., Blackshear, J.L., Shen, W.K., Hammill, S.C., Gersh, B.J., 2001. Epidemiology and natural history of atrial fibrillation: clinical implications. J. Am. Coll. Cardiol. 37, 371–378.

Danthi, S., Enyeart, J.A., Enyeart, J.J., 2004. Caffeic acid esters activate TREK-1 potassium channels and inhibit depolarization-dependent secretion. Mol. Pharmacol. 65, 599–610.

Decher, N., Kumar, P., Gonzalez, T., Pirard, B., Sanguinetti, M.C., 2006. Binding site of a novel Kv1.5 blocker: a foot in the door against atrial fibrillation. Mol. Pharmacol. 70, 1204–1211.

Decher, N., Pirard, B., Bundis, F., Peukert, S., Baringhaus, K.H., Busch, A.E., Steinmeyer, K., Sanguinetti, M.C., 2004. Molecular basis for Kv1.5 channel block: conservation of drug binding sites among voltage-gated K^+ channels. J. Biol. Chem. 279, 394–400.

Fedida, D., Wible, B., Wang, Z., Fermini, B., Faust, F., Nattel, S., Brown, A.M., 1993. Identity of a novel delayed rectifier current from human heart with a cloned K^+ channel current. Circ. Res. 73, 210–216.

Glitsch, M.D., Bakowski, D., Parekh, A.B., 2002. Effects of inhibitors of the lipo-oxygenase family of enzymes on the store-operated calcium current I_{CRAC} in rat basophilic leukaemia cells. J. Physiol. 539, 93–106.

Hatton, C.J., Peers, C., 1997. Multiple effects of nordihydroguaiaretic acid on ionic currents in rat isolated type I carotid body cells. Br. J. Pharmacol. 122, 923–929.

Herrera, D., Mamarbachi, A., Simoes, M., Parent, L., Sauve, R., Wang, Z., Nattel, S., 2005. A single residue in the S6 transmembrane domain governs the differential flecainide sensitivity of voltage-gated potassium channels. Mol. Pharmacol. 68, 305–316.

Honore, E., Barhanin, J., Attali, B., Lesage, F., Lazdunski, M., 1994. External blockade of the major cardiac delayed-rectifier K^+ channel (Kv1.5) by polyunsaturated fatty acids. Proc. Natl. Acad. Sci. U. S. A. 91, 1937–1944.

Jager, H., Grissmer, S., 2001. Regulation of a mammalian Shaker-related potassium channel, hKv1.5, by extracellular potassium and pH. FEBS. Lett. 488, 45–50.

Knobloch, K., Brendel, J., Peukert, S., Rosenstein, B., Busch, A.E., Wirth, K.J., 2002. Electrophysiological and antiarrhythmic effects of the novel I(Kur) channel blockers, S9947 and S20951, on left vs. right pig atrium in vivo in comparison with the I(Kr) blockers dofetilide, azimilide, d,l-sotalol and ibutilide. Naunyn. Schmiedebergs Arch. Pharmacol. 366, 482–487.

Korn, S.J., Horn, R., 1990. Nordihydroguaiaretic acid inhibits voltage-activated Ca^{2+} currents independently of lipoxygenase inhibition. Mol. Pharmacol. 38, 524–530.

Kyte, J., Doolittle, R.F., 1982. A simple method for displaying the hydropathic character of a protein. J. Mol. Biol. 157, 105–132.

Lagrutta, A., Wang, J., Fermini, B., Salata, J.J., 2006. Novel, potent inhibitors of human Kv1.5 K^+ channels and ultrarapidly activating delayed rectifier potassium current. J. Pharmacol. Exp. Ther. 317, 1054–1063.

Li, G.R., Feng, J., Yue, L., Carrier, M., Nattel, S., 1996. Evidence for two components of delayed rectifier K^+ current in human ventricular myocytes. Circ. Res. 78, 689–696.

Long, S.B., Campbell, E.B., Mackinnon, R., 2005. Crystal structure of a mammalian voltage-dependent Shaker family K^+ channel. Science 309, 897–903.

Mackinnon, R., Yellen, G., 1990. Mutations affecting TEA blockade and ion permeation in voltage-activated K^+ channels. Science 250, 276–279.

Meves, H., 1994. Modulation of ion channels by arachidonic acid. Prog. Neurobiol. 43, 175–186.

Perchenet, L., Clement-Chomienne, O., 2000. Characterization of mibefradil block of the human heart delayed rectifier hKv1.5. J. Pharmacol. Exp. Ther. 295, 771–778.

Rezazadeh, S., Claydon, T.W., Fedida, D., 2006. KN-93 (2-[N-(2-hydroxyethyl)]-N-(4-methoxybenzenesulfonyl)]amino-N-(4-chlorocinnamyl)-N-methylbenzylamine), a calcium/calmodulin-dependent protein kinase II inhibitor, is a direct extracellular blocker of voltage-gated potassium channels. J. Pharmacol Exp. Ther. 317, 292–299.

Roden, D.M., 2001. Pharmacogenetics and drug-induced arrhythmias. Cardiovasc. Res. 50, 224–231.

Simard, C., Drolet, B., Yang, P., Kim, R.B., Roden, D.M., 2005. Polymorphism screening in the cardiac K^+ channel gene KCNA5. Clin. Pharmacol. Ther. 77, 138–144.

Snyders, D.J., Yeola, S.W., 1995. Determinants of antiarrhythmic drug action. Electrostatic and hydrophobic components of block of the human cardiac hKv1.5 channel. Circ. Res. 77, 575–583.

Stump, G.L., Wallace, A.A., Regan, C.P., Lynch Jr., J.J., 2005. In vivo antiarrhythmic and cardiac electrophysiologic effects of a novel diphenylphosphine oxide IKur blocker (2-isopropyl-5-methylcyclohexyl) diphenylphosphine oxide. J. Pharmacol. Exp. Ther. 315, 1362–1367.

Trotter, B.W., Nanda, K.K., Kett, N.R., Regan, C.P., Lynch, J.J., Stump, G.L., 2006. Design and synthesis of novel soquinoline-3-nitriles as orally bioavailable Kv1.5 antagonists for the treatment of atrial fibrillation. J. Med. Chem. 49, 6954–6957.

Valenzuela, C., Delpón, E., Franqueza, L., Gay, P., Pérez, O., Tamargo, J., Snyders, D.J., 1996. Class III antiarrhythmic effects of zatebradine. Time-, state-, use-, and voltage-dependent block of hKv1.5 channels. Circulation 94, 562–570.

Varro, A., Biliczki, P., Iost, N., Virag, L., Hala, O., Kovacs, P., Matyus, P., Papp, J.G., 2004. Theoretical possibilities for the development of novel antiarrhythmic drugs. Curr. Med. Chem. 11, 1–11.

Wang, Z., Estacion, M., Mordan, L.J., 1993a. Ca^{2+} influx via T-type channels modulates PDGF-induced replication of mouse fibroblasts. Am. J. Physiol. 265, C1239–C1246.

Wang, Z., Fermini, B., Nattel, S., 1993b. Sustained depolarization-induced outward current in human atrial myocytes: evidence for a novel delayed rectifier K^+ current similar to Kv1.5 cloned channel currents. Circ. Res. 73, 1061–1076.

Wang, Z., Hesketh, J.C., Fedida, D., 2000. A high-Na^+ conduction state during recovery from inactivation in the K^+ channel Kv1.5. Biophys. J. 79, 2416–2433.

Yamamura, H., Nagano, N., Hirano, M., Muraki, K., Watanabe, M., Imaizumi, Y., 1999. Activation of Ca^{2+}-dependent K^+ current by nordihydroguaiaretic acid in porcine coronary arterial smooth muscle cells. J. Pharmacol. Exp. Ther. 291, 140–146.

Yeola, S.W., Rich, T.C., Uebele, V.N., Tamkun, M.M., Snyders, D.J., 1996. Molecular analysis of a binding site for quinidine in a human cardiac delayed rectifier K^+ channel. Role of S6 in antiarrhythmic drug binding. Circ. Res. 78, 1105–1114.